Thermal Science and Engineering Progress 67 (2025) 104142

Contents lists available at ScienceDirect

Thermal Science and Engineering Progress

journal homepage: www.sciencedirect.com/journal/thermal-science-and-engineering-progress

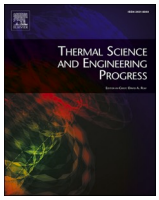

Dry-out vapor quality incipience in flow boiling: Empirical correlation development with particle Swarm algorithm

Nima Irannezhad, Luisa Rossetto, Andrea Diani *

Department of Industrial Engineering, University of Padova, Italy

ARTICLE INFO

Keywords:
Dry-out
Flow boiling
Particle Swarm Algorithm
Empirical Correlation

ABSTRACT

With the growing demand for electronic cooling, flow boiling has emerged as a critical mechanism in modern thermal systems. Considering the complexity of flow boiling mechanism, which is influenced by many parameters such as operating conditions, tube geometry, type of refrigerant and other factors, predicting parameters such as critical heat flux and vapor quality at the incipience of dry-out is rather challenging and often requires high computational effort. Concluding a comprehensive review of studies on flow boiling dry-out, the current article garners 418 data points regarding vapor quality at the incipience of dry-out in flow boiling of refrigerants inside tubes, with diameters from 0.6 to 6 mm. Heat fluxes, mass fluxes and reduced pressures in the database ranged from 5 to 400 kW m^{-2}, 150 to 1500 kg m^{-2} s^{-1} and 0.1 to 0.9 respectively. Utilizing the Particle Swarm Algorithm and seven dimensionless numbers which influence the flow boiling mechanism, a new empirical correlation is proposed which can achieve an accuracy of 15.9 % mean average error. A secondary database comprised of 133 data points is also collected for validation of the model. The proposed model of vapor quality at the incipience of dry-out is considerably accurate and facilitates the predictions of dry-out for tubes with inner diameter between 0.6 mm and 3 mm.

1. Introduction

High heat flux removal is a very relevant factor in the design of several systems such as high-performance computer chips, laser diodes, fission reactors and future nuclear fusion systems. New technical applications in the electronic industry, for example, demand high-heat flux dissipation from small areas. Micro and minichannels are well suited to accomplish this task, as they provide large heat transfer per surface area. Therefore, boiling in minichannels is a common application in compact heat exchangers for emerging technologies. It also presents strong potential for improving refrigeration and air-conditioning systems, since it allows reducing the inventory charge and air-side pressure drop.

In recent years, attention has been paid to the study of two-phase flow and boiling heat transfer in minichannels. The thermal crisis, as well, has received much attention in literature owing to the great importance since the performance of heat transfer equipment is severely affected by the inception of thermal crisis. The liquid next to the wall is replaced by vapor and a sharp decrease in the heat transfer coefficient follows. When the heat flux is imposed, such phenomenon causes a sudden large increase in the temperature of the surface on which evaporation is occurring, and it can lead to system failure. Understanding the onset and development of dryout helps in predicting critical heat flux (CHF) and allows engineers to set operational limits that prevent material degradation and system instability. Moreover, accurate dryout modeling is essential for optimizing channel geometry and refrigerant flow distribution in compact and high-heat flux applications.

This heat transfer deterioration takes place with drastically different mechanisms under subcooled or saturated flow boiling conditions. For subcooled or low-quality saturated flow boiling conditions, the main boiling mechanism is nucleate boiling, and the onset of the thermal crisis follows the departure from nucleate boiling. In saturated annular flow boiling conditions, dry-out of the film adjacent to the heated wall is the trigger mechanism for the thermal crisis (Celata et al. [1]). While the two mechanisms are distinctively diverse, both incorporate the term ‘critical heat flux condition’ to give a general description of the phenomenon and the term ‘critical heat flux’ (CHF) to refer to the heat flux value at which the reduction of the heat transfer coefficient takes place (Collier and Thome [2]).

As the phenomenon of heat transfer crisis is extremely complex, there is no satisfactory explanation of the dependence of crisis from the flow boiling parameters. The prediction of dry-out relies on empirical

* Corresponding author at: Department of Industrial Engineering, University of Padova, Via Venezia 1, 35131 Padova, Italy.
E-mail address: andrea.diani@unipd.it (A. Diani).

https://doi.org/10.1016/j.tsep.2025.104142
Received 14 April 2025; Received in revised form 1 September 2025; Accepted 22 September 2025
Available online 22 September 2025

Nomenclature

Abbreviations

Al	Aluminum
ANN	Artificial neural network
CHF	Critical heat flux, W m^{-2}
Cu	Copper
MAE	Mean average error, $\sum \left[abs\left(\frac{x_{di,pred}-x_{di,exp}}{x_{di,exp}} \right) \right] /n \times 100$
MC	Multiport of circular section
ML	Machine learning
RMSE	Root mean squared error, $\sqrt{\sum \left(x_{di,pred} - x_{di,exp} \right)^2 /n}$
SC	Single tube of circular section
SR	Single tube of rectangular section
SS	Stainless steel

Greek letters

μ	Viscosity, Pa s
ρ	Density, kg m^{-3}
σ	Surface tension, N m^{-1}

Physical parameters

x	Vapor quality
g	Gravity, m s^{-2}
G	Mass flux, kg m^{-2} s^{-1}
h_{lv}	Latent heat of vaporization, J kg^{-1}
L	Length, m
P	Pressure, Pa
q	Heat flux, W m^{-2}
T	Temperature, °C

Dimensionless

Bo	Boiling number
Ca	Capillary number
Co	Confinement number
Fr	Froude number
P_{red}	Reduced pressure
We	Weber number

Subscripts

crit	critical
di	Dryout incipience
exp	experimental
h	hydraulic
L, l	Liquid phase
pred	predicted
sat	saturation
V, G, v	Vapor phase

Table 1
Classification of tubes.

Kandlikar and Grande [4]	MOLECULAR NANOCHANNEL	$D_h < 0.1$ μm
	TRANSITIONAL NANOCHANNEL	$0.1 < D_h < 1$ μm
	TRANSITIONAL MICROCHANNEL	$1 < D_h < 10$ μm
	MICROCHANNEL	$10 < D_h < 200$ μm
	MINICHANNEL	200 μm $< D_h <$ 3 mm
	CONVENTIONAL CHANNEL	$D_h > 3$ mm
Mehendale et al. [5]	MICROCHANNEL	$1 < D_h < 100$ μm
	MESO-CHANNEL	100 μm $< D_h <$ 1 mm
	COMPACT PASSAGE	$1 < D_h < 6$ mm
	CONVENTIONAL CHANNEL	$D_h > 6$ mm
Kew and Cornwell [6]	The transition from macro to micro size channel varies with fluid and reduced pressure (confinement number)	$Co = \frac{1}{D_h}\sqrt{\frac{\sigma}{g(\rho_L - \rho_G)}} = 0.5$
Triplett et at. [7]	The transition from macro to micro size channel varies with fluid and reduced pressure (Laplace Constant)	$D_h = \sqrt{\frac{\sigma}{g(\rho_L - \rho_G)}}$
Brauner and Moalem-Maron [8]	The transition from macro to micro size channel varies with fluid and reduced pressure (Etwös number)	$Eö = \frac{g(\rho_L - \rho_G)D_h^2}{(2\pi)^2\sigma} = 1$
Ullmann and Brauner [9]	The transition from macro to micro size channel varies with fluid and reduced pressure	$\frac{g(\rho_L - \rho_G)D_h{}^2}{\sigma} = 1.6$
Akbar et al. [10]	Buoyancy effect is negligible for Bond number less than 0.3. Transition to microchannels	$Bo = \sqrt{\frac{g(\rho_L - \rho_G)D_h{}^2}{\sigma}} = 0.3$
Qu and Mudawar [11]	MINICHANNELS	$1 < D_h < 3$
	MICROCHANNELS	$D_h < 1$ mm

correlations derived from experimental databases.

Since flow boiling heat transfer and transport phenomena in small hydraulic diameter channels are quite different from those in macro channels (Cheng and Mewes [3]), the first issue to clarify is the distinction from small and normal size channels. At present though there is no well-established criterion to describe the transition from macro traditional channels to micro scale channels. Table 1 reports some recent classifications.

For Kandlikar and Grande [4], considering engineering practice, conventional channels are identified as those with a hydraulic diameter larger than 3 mm. The compact heat exchangers passages with a hydraulic diameter range between 200 μm and 3 mm have been classified as minichannels. The microchannel presents smaller diameter.

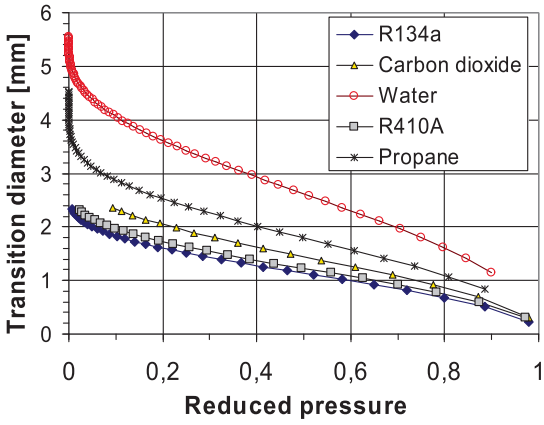

Fig. 1. Transition diameter (from macro to micro) versus reduced pressure [6].

Mehendale et al. [5] classification is also based on the hydraulic diameter value (Table 1); for them mini channels have diameters smaller than 6 mm.

For Qu and Mudawar [11] the channels are mini with cross sectional dimensions from 1 to 3 mm while they are micro with the same dimensions less than 1 mm.

The two-phase flow in channels is influenced by gravity, surface tension, viscosity and inertia forces effects. Since in small horizontal channels gravity forces should lose importance at the expense of surface tension, some criterions employ the comparison between the two forces.

Kew and Cornwell [6] proposed an approximate physical criterion based on the confinement number, Co (Table 1), to guide channel size selection. They observed that correlations developed for conventional channels perform poorly when applied to channels with confinement numbers around 0.5 and above. Unlike the fixed 3 mm threshold of

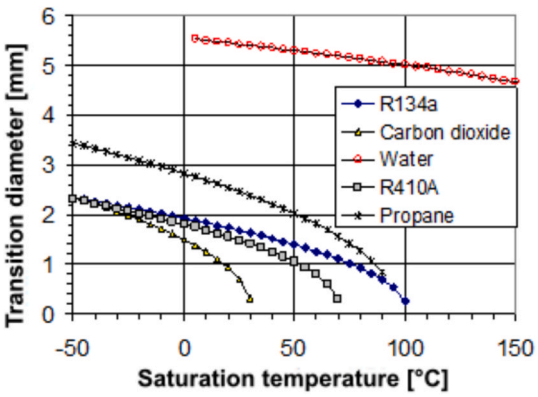

Fig. 2. Transition diameter (from macro to micro) versus temperature [6].

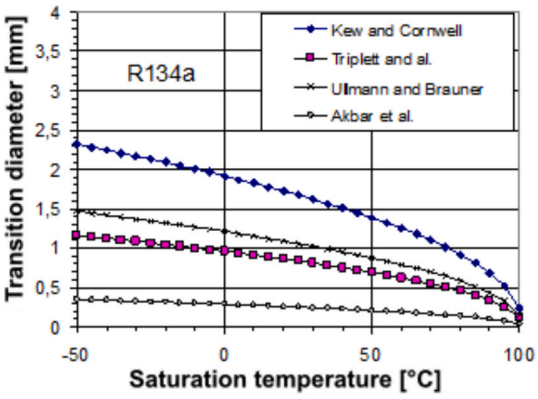

Fig. 3. Transition diameter (from macro to micro) versus temperature for R134a according to various models.

Kandlikar and Grande [4], the transition diameter in Kew and Cornwell [6] depends on fluid and reduced pressure. It may reach 5 mm for water at low reduced pressure and fall below 1 mm for CO_2 at reduced pressures above 0.8, as shown in Fig. 1. Fig. 2 shows the transition diameter versus saturation temperature for R134a.

Triplett et al. [7] and Brauner and Moalem-Maron [8] proposed similar criteria with different transition diameters (Table 1). Ullmann and Brauner [9], on the basis of flow pattern maps, proposed a new threshold diameter for microscale effects which is 63 % of the Kew and Cornwell value.

Akbar et al. [10] stated that buoyancy effect can be negligible for Bond number less than 0.3. Fig. 3 shows the transition diameters for R134a, following Kew and Cornwell [6], Triplett et al. [7], Ullmann and Brauner [8] and Akbar et al. [10].

Celata [12] points out that bubble size is affected by the gravity level but this functional dependence is also interrelated with vapour quality (flow pattern and heat transfer regime) and with fluid velocity (drag force). Therefore, he suggests that a further parameter such as drag force has to be taken into account for a wider validity of threshold identification.

Given the non-unanimous tube classifications, flow regime studies help clarify flow boiling behavior. Pettersen [13] examined CO_2 vaporization at 0–20 °C in a 0.98 mm tube with $q = 13$ kW m^{-2}, mass flux 100–580 kg m^{-2} s^{-1}, and vapor quality 0.12–0.99. Wavy annular flow dominated, with droplet entrainment at high temperature and low surface tension; intermittent regimes appeared at low mass flux and vapor quality, while stratified flow was absent. The intermittent–annular transition ($10 < We_G < 45$) matched the Akbar et al. [10] map for air–water sub-millimeter tubes. Yun and Kim [14] visualized CO_2 boiling in a rectangular channel (16 mm × 2 mm) under 0–250 kW m^{-2} heat flux, 217–868 kg m^{-2} s^{-1} mass flux, and vapor quality up to 0.8. Regimes included bubbly, intermittent, and annular flow, with droplet entrainment; the slug–annular transition occurred at $We_G < 20$. Saitoh et al. [15] reported only annular and intermittent flows during R134a boiling in 0.51–3.1 mm tubes, with 5–39 kW m^{-2} heat flux, 100–450 kg m^{-2} s^{-1} mass flux, and reduced pressures 0.12–0.91. Chen et al. [16] studied vertical upward boiling of R134a in 1.1–4.26 mm tubes, observing dispersed bubble, bubbly, confined bubble, slug, churn, annular, and mist flow; confined bubbles appeared only in the 1.1 mm tube at 0.6–1.4 MPa. These findings highlight that dry-out depends on geometry, refrigerant properties, mass and heat fluxes, and saturation pressure, requiring a holistic view to identify parameters governing its onset.

1.1. Impact of reduced pressure

Various experimental articles have studied the impact of saturation pressure on the vapor quality and critical heat flux at the onset of dry-out. A comprehensive analysis of the works reveals that unanimous observation does not exist regarding the relationship between the pressure and dry-out conditions.

Anwar et al. [17], tested R152a in vertical mini-channel for two saturation temperatures of 27 °C and 32 °C; no noticeable difference was seen in critical heat flux and vapor quality at the incipience of dry-out at the two pressures. However, authors commented that at higher pressures due to higher vapor densities and consequent lower vapor velocity, the destruction of liquid thickness is expected to be delayed. Within the testing conditions of Arcasi et al. [18] for R454C, at two saturation pressures of 16 and 20 bar the vapor quality at the incipience of dry-out has a comparable value.

On the contrary to the previous assertion, Pysz et al. [19], reports an inverse relationship between vapor quality at the incipience of dry-out and the saturation pressure, attributing it to the reasoning of Marchetto et al. [20] where higher pressures cause lower surface tension forces which contribute to the instability of the liquid thickness. Similarly, for R245fa inside a 3 mm ID tube over large saturation pressure ranges, Charnay et al. [21] records dry-out that takes place sooner as the pressure increases. Furthermore, in their holistic review of articles with medium to high reduced pressure, the authors express a one-sided opinion on the inverse correlation between reduced pressure and vapor quality despite two known articles [22,23] where the opposite is seen.

Overall, it can be assumed that the relationship between pressure and vapor quality at which dry-out takes place is ultimately decided by the interaction between two forces that are inversely influenced by pressure. The stabilizing component, which is the surface tension force, lowers with higher pressures and the destructive force of shear-stress also lowers due to reduction of vapor velocity at higher pressures.

1.2. Impact of mass flux

Considering the findings within the literature, it could be stated that given the conflicting results, the impact of mass flux cannot be correlated with the dry-out condition in a straightforward way. Testing two refrigerants in two different experimental campaigns (R454A, R290) inside a tube of 6 mm ID, Mastrullo et al. [24] and Lillo et al. [25] observed no noticeable variation in occurrence of dry-out with changes in mass flux, while, with smaller diameters of 1 and 2 mm and higher pressures with R744, Jiang et al. [26] reported that the dry-out occurs much sooner with higher mass fluxes due to presence of limited liquid thickness under the influence of elevated shear-stress forces.

Paradoxically in a single article of Ducoulombier et al. [27] focused on studying flow boiling of CO_2 inside a tube of 0.529 mm ID for two saturation temperatures of −10 and −5°C, a delayed dry-out with higher mass fluxes is recorded, whereas for the 0 °C the contrary occurs.

The impact of mass flux on dry-out occurrence cannot be reduced to a

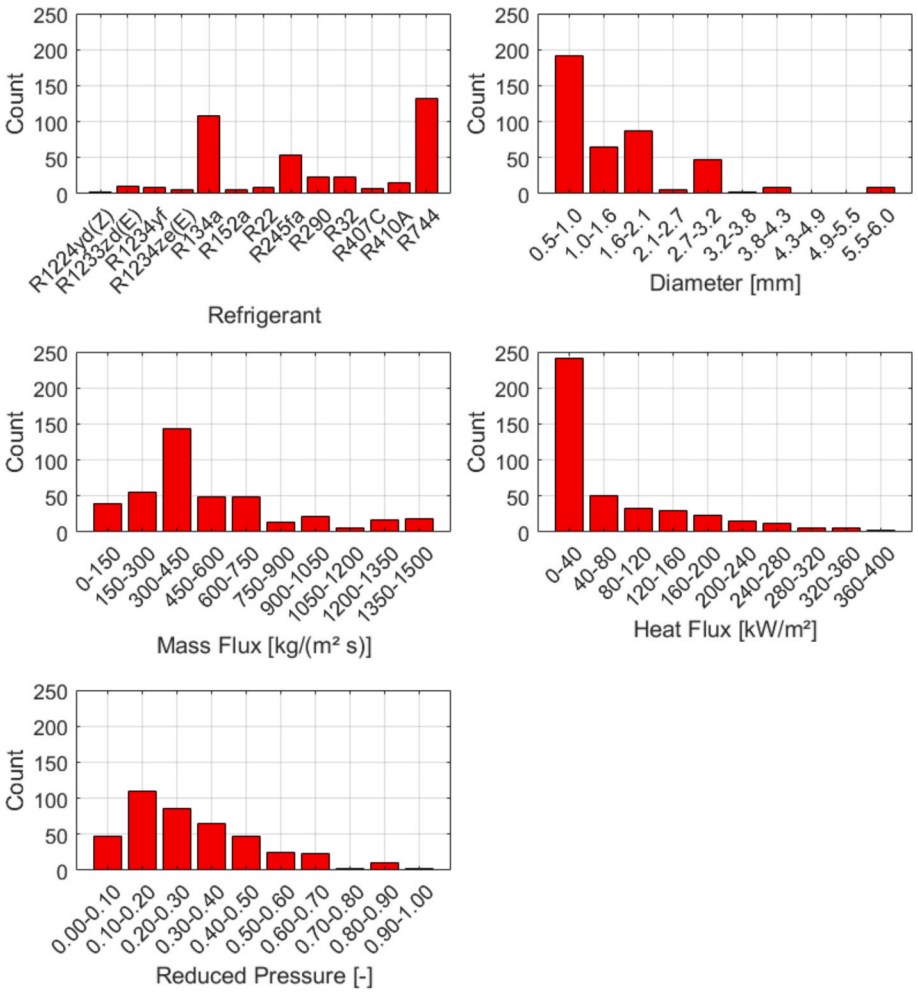

Fig. 4. Distribution of data implemented for modelling.

simple linear relationship as with variation of other parameters the relationship can be completely inversed.

1.3. Impact of tube diameter

The previously given definitions on micro and mini specifications of tube geometries demonstrate the importance of the geometrical features in flow boiling mechanism. In detail, it is the combination of operating conditions with the diameter that can greatly vary the results. However, a general comment can be made for what concerns the occurrence of dry-out; under the same conditions, the increase in diameter will delay the dry-out (assuming the flow regime is always annular) due to reduced shear-stress forces that entrain the liquid thickness on the walls.

Considering the abovementioned aspect, Saitoh et al. [28] examine the accuracy of correlations comparing predictions with their experimental data with various tube diameters, realizing the incapability of models in providing decent predictions for diameters 1.12 and 0.5 mm. They have proposed a new model which shows to have a direct relationship between diameter and the incipience of dry-out with a logarithmic growth. The experimental study of Ali and Palm [29] confirms the direct relation between the tube diameter and dry-out incipience where between the two tubes of 1.70 mm and 1.22 mm under equal conditions dry-out occurred later in the latter case.

In spite of the previous finding, it is of high importance to identify the flow pattern before establishing any *a priori* relation between the diameter of vapor quality at dry-out incipience. The exemplary work of Ong and Thome [30] on flow pattern predictions is noteworthy in which the authors claim that the confinement numbers of 0.4 and 1 perfectly define the range of microscale tubes as for values beyond 1 the gravity force proves to be completely ineffective and for values of below 0.4 it becomes a dominant force. It can be said that a direct correlation can be assumed between diameter and vapor quality at the incipience of dry-out for micro-scale tubes.

Given the complexity and interconnectedness of the parameters influencing the dry-out mechanism, the current paper collects a database composed of 418 experimental points of significantly different operating conditions, geometries and refrigerants and, by implementing dimensionless parameters encompassing all known parameters influencing the occurrence of dry-out, provide a generalized model.

1.4. Research gap

Being aware of the dichotomy that exists in two-phase flow patterns for tubes of different category (mini, micro, macro) the modelling procedure is forced to provide two different correlations for the vapor quality at the incipience of dry-out based on the confinement number which is utilized by various authors in recent years. To ensure that the empirical model is truly representing a physical correlation between the inputs and the output, pre-defined relationships between the parameters and the dry-out vapor quality are given and the optimization algorithm of particle swarm is forced to find a suitable power function under such *a priori* relationship. It should be noted that the benefits of implementing the particle swarm algorithm in the current context are explored for the first time. Moreover, to make sure that the correlation discovered by the

Table 2
Modelling database.

Author	Channel	d_h [mm]	Fluid	p_{RED}*	G [kg m^{-2} s^{-1}]	Heating Mode	q [kW m^{-2}]	L [m]	Tube	Uncertainty x, G, q
Pettersen [31]	MC	0.8	CO_2	0.472 – 0.872	190 – 570	Water	10 – 20	0.54	AL	±13 %, ±3%, ±8.5 %
Gasche [32]	SR.	0.8	CO_2	0.838	58 – 235	Electr.	1.8		AL-Glass	±10 %, ±5%, ±3%
Yun et al. [15]	SC	2	CO_2	0.538	1000 – 1500	Electr.	7.2 – 46	0.4	SS	±4%, ±0.2 %, ±5%
Choi et al. [33]	SC	1.5 – 3	CO_2	0.412 – 0.610	200 – 600	Electr.	20 – 40	2–3	SS	±9.7 %, ±9.5 %, ±2.7 %
Hihara and Dang [34]	SC	1 – 2	CO_2	0.689	360 – 1440	Electr.	4.5 – 36			–
Saitoh et al. [15]	SC	3.1	R134a	0.086 – 0.120	300	Electr.	12 – 14	0.55–3.235	SUS 304	–
Saitoh et al. [28]	SC	1.12, 2, 3.1	R134a	0.12, 0.74, 0.91	100 – 400	Electr.	5 – 29	0.55–3.235	SUS 304	–
Pamitran et al. [35]	SC	1.5 – 3.0	R410A R407C	0.146 – 0.222	300 – 600	Electr.	5 – 15	1.5–3	SS	–
Jiang et al. [26]	SC	1–2	CO_2	0.358 – 0.68	50 – 1350	Electr.	2 – 35	0.3	SS	±6%, ±0.12 %, ±2.33 %
Marchetto et al. [36]	SC	2	R1233zd(E) R245fa	0.15 – 0-25	375	Electr.	36 – 54	0.125	SS	±0.035, ±4.6 %, ±6.5 %
Charnay et al. [37]	SC	3	R245fa		700	Electr.	30 – 90	–	SS	±0.015, ±5%, ±3%
Son and Oh [38]	SC	3.36, 1.77, 5.35	R22, R134a	0.11, 0.086	200 – 400	Water	10 – 30	–	Cu	–
Charnay et al. [21]	SC	3	R245fa	0.21 – 0.52	300 – 1000	Electr.	10 – 50	0.185	SS	±0.015, ±2%, ±4%
Del Col and Bortolin [39]	SC	0.96	R245fa, R134a, R32	0.04 – 0.33	100 – 1000	Water	10 – 250	0.097–0.202	Cu	±0.007, ±0.2 %, ±8%
Wu et al. [40]	SC	1.42,	CO_2	0.136 – 0.472	300 – 600	Electr.	7.5 – 29.8	0.150	SS	±2%, ±2%, ±1. 2 %
Ali and Palm [29]	SC	1.22,1.70	R134a	0.17 – 0.2	50 – 600	Electr.	18 – 156	0.220	SS	±4%, ±2%,±3%
Lillo et al. [25]	SC	6	Propane	0.22 – 0.28	150 – 300	Electr.	10 – 40	0.146	SS	±0.03, ±1.4 %, ±0.68 %
Zhao et al. [41]	SC	4	R1233zd(E), R1224yd, R245fa, HFE347pc-f	0.06 – 0.13	30 – 50	Electr.	5 – 14	–	SS	±11 %, ±0.3 %, ±0.5 %
Anwar et al. [42]	SC	1.6	R1234yf	0.21 – 0.24	100 – 500	Electr.	50 – 125	0.245	SS	–, ±3.5 %, ±4%
Maqbool et al. [43]	SC	1.7, 1.224	Propane	0.21 – 0.34	100 – 500	Electr.	60 – 210	0.245	SS	±5%, ±3.5 %, ±2%
Anwar et al. [17]	SC	1.6	R152a	0.13	100 – 500	Electr.	40 – 240	0.245	SS	–, ±2%, ±1.5 %
Ducoulombier et al. [27]	SC	0.596	CO_2	0.35 – 0.47	200 – 1400	Electr.	10 – 30	0.159	SS	±0.8 %, ±1.9 %, ±1.5 %

SC single tube of circular section
SR single tube of rectangular section
MC multiport of circular section
SS stainless steel; Al Aluminum; Cu copper.
– Not reported.
* $P_{RED} = \frac{p_{sat}}{p_{crit}}$.

optimization algorithm is representative of the physical phenomena, the correlation is tested on a secondary database (133 data points) which is not utilized during the modelling phase of the algorithm.

2. Database

Being aware of the significant impact of operating conditions, refrigerant, heat flux, geometrical features and other parameters, this paper aims to collect a comprehensive database of different parameters to ensure that the predictive model to be generated by the data is suitable for a wide range of conditions.

For a clearer description, the range of reduced pressure, mass flux, heat flux, diameter and the name of refrigerants are all provided in Fig. 4.

Furthermore, to provide more complete information on the articles from which the data are extracted, Table 2 gives comprehensive information regarding the test section and the experimental uncertainties reported by the authors.

Considering the many nuances that exist at low diameters and high reduced pressure, the current database meets the authors' goal of providing a model that can capture the right relationship between the inputs and the dry-out vapor quality. At least 20 points, relative to CO_2 flow boiling, in the database have reduced pressures substantially close to the critical conditions. The range of diameters within the database corresponds to maximum and minimum confinement numbers of 2 and 0.2 respectively. Overall, the number of data points is 418.

The identification of dry-out vapor quality was conducted based on either sharp decrease in heat transfer coefficient or the sudden rise of surface temperature. To better comprehend how such points are identified, a figure belonging to exemplary experimental campaigns is given (see Fig. 5). Furthermore, to quantitatively express this reduction, we considered a data point to be the onset of dryout only if the increase in vapor quality resulted in a 30–60 % reduction in the heat transfer coefficient. However, it should be noted that the magnitude of the reduction for different diameters, saturation pressures, refrigerants, heat fluxes, and mass fluxes is quite variable, making the situation quite subjective and difficult to clearly quantify. However, this subjectivity cannot significantly impact the identification process, since even with a

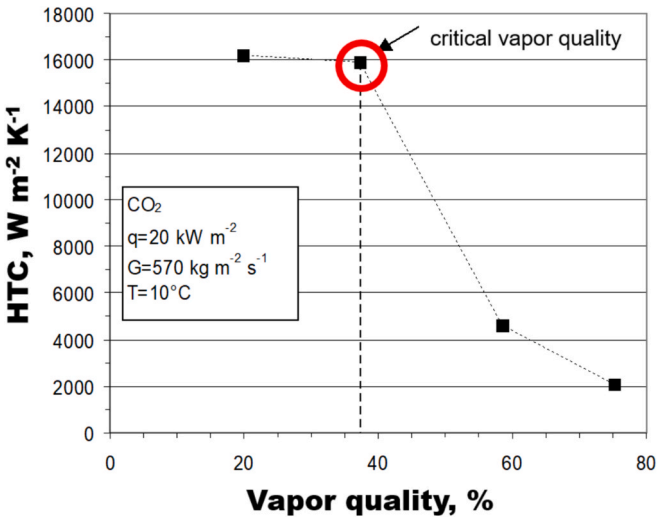

Fig. 5. Identification of critical vapor quality with sharp reduction in heat transfer coefficient (until now referred to as vapor quality at the incipience of dry-out).

qualitative assessment, the trend contributes to determining the vapor quality at the onset of dryout.

From the uncertainties reported in Table 2, perhaps the most important one is the one assigned to vapor quality which directly impacts the accuracy of the models that are built on the database. Considering the unavailability and the unlikelihood of finding a dryout database with low and similar errors in measurements, it is necessary to conduct an uncertainty propagation analysis for a correlation built on the database.

3. Current correlations

3.1. Empirical correlations

To assess whether the current correlations provide a satisfactory prediction of vapor quality at the incipience of dry-out for the gathered database, three current promising models are tested.

Kim and Mudawar [44], garnering a large database comprised of 997 experimental points of vapor quality at the incipience of dry-out in mini/micro channels, composed a predictive model which yielded a mean average error (MAE) of 12.5 % for the entire database. Since authors noted the forces of inertia, viscous forces and surface tension to influence the boiling mechanism, their empirical formula takes into consideration the following parameters as their representatives:

$$\mathrm{We_L} = \frac{G^2 \bullet D_h}{\rho_L \bullet \sigma} \tag{1}$$

$$\mathrm{Ca} = \frac{We_L}{Re_L} \tag{2}$$

$$\mathrm{Bo} = \frac{q}{G \bullet h_{lv}} \tag{3}$$

which resulted in the development of the final equation given as:

$$x_{di} = 1.4\mathrm{We_L^{0.03}} \bullet P_{RED}^{0.08} - 15.0\left(\mathrm{Bo} \bullet \frac{P_H}{P_F}\right)^{0.15} \bullet \mathrm{Ca}^{0.35} \bullet \left(\frac{\rho_g}{\rho_L}\right)^{0.06} \tag{4}$$

P_H is the perimeter involved in the heat transfer process, whereas P_F is the perimeter involved in the fluid flow.

Cheng et al. [45] aiming to improve a pre-existing model of two-phase flow pattern, extract the following expression for the vapor quality at the incipience of dry-out which proved to have predicted the flow patterns of CO_2 inside a channel of 0.8 mm. However, it must be

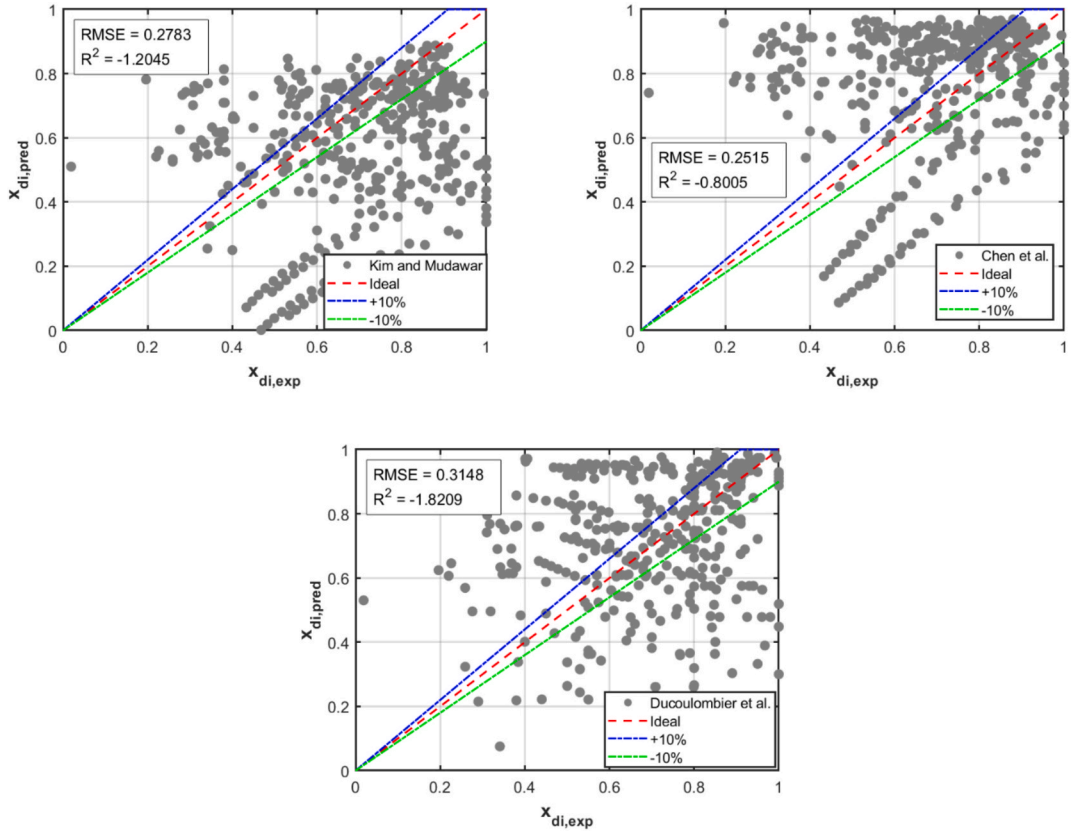

Fig. 6. Predicted values of vapor quality at the incipience of dry-out versus experimental measurements of the gathered database by three models.

Table 3
Mean Average Error of predictions made by models over the database.

	MAE*			Limitations
Model	Overall	$P_{RED} < 0.5$, $P_{RED} > 0.5$	$0.4 < Co < 1$	
Kim and Mudawar	40.6 %	40.1 %, 43.3 %	31.0 %	data at low reduced pressure
Cheng et al	40.5 %	42.2 %, 37.0 %	31.0 %	data with small diameters
Ducolumbier et al.	41.6 %	37.3 %, 67.1 %	35.3 %	Effect of mass flux
	$x_{di} - x_{exp}$			
Kim and Mudawar	0.21	0.21, 0.22	0.18	
Cheng et al	0.20	0.21, 0.15	0.18	
Ducolumbier et al.	0.20	0.17, 0.37	0.20	

* $MAE = \sum \left[abs\left(\frac{x_{di,pred} - x_{di,exp}}{x_{di,exp}} \right) \right] / n \times 100.$

noted that none of the flow patterns were in dry-out region. The expression provided by the authors is given as:

$$x_{di} = 0.58e^{\left[0.52-0.236We_V^{0.17}\bullet Fr_{V,Mori}^{0.17}\bullet\left(\frac{\rho_V}{\rho_L}\right)^{0.25}\bullet\left(\frac{q}{q_{crit}}\right)^{02.7}\right]} \quad (5)$$

$$We_V = \frac{G^2 \bullet D_h}{\rho_V \bullet \sigma} \quad (6)$$

$$Fr_{Vo,Mori} = \frac{G^2}{\rho_V(\rho_L - \rho_V)g \bullet D_h} \quad (7)$$

$$q_{crit} = 0.131\rho_V^{0.5} \bullet h_{lv}[g \bullet \sigma(\rho_L - \rho_V)]^{0.25} \quad (8)$$

Ducoulombier et al. [27] in an experimental study of CO_2 flow boiling inside a mini channel of 0.5 mm inner diameter (mass fluxes were varied between 200–1200 kg m^{-2} s^{-1}) stated to have observed the same unusual trend of mass flux versus vapor quality at the dry-out incipience which was previously witnessed by other authors such as Yun and Kim [46] where the dry-out is delayed with augmentation of mass flux. After testing saturation temperatures of −10, −5 and 0 °C, they have suggested a new model for the dry-out incipience vapor quality that accounts for this behavior. The authors argued that the reasoning behind this behavior is still unclear and needs to be corroborated. Their expression for dry-out which has a direct relation to the mass flux is given as:

$$x_{di} = 1 - 338Bo^{0.703} \bullet P_{RED}^{1.43} \quad (9)$$

The accuracies of the models on our current database are plotted in Fig. 6. In detail the values of the mean absolute error, MAE, expressed in percentage are reported in Table 3 for all the data points (overall MAE). In the same Table 3 to delve into the predictive capacity of the models, the specific MAEs are given for data with Confinement number between 0.4 and 1 (corresponding to the micro classification of [30]). Furthermore, since the inaccuracy of a predictive model could stem from a change in the physical phenomena influenced by variations of pressure, the MAEs for data with reduced pressure below and higher than 0.5 are given as well. As can be seen from the predictions, the models do not provide satisfactory results despite their previous promising predictions on their own database. Same concept is applied to absolute errors of predictions in Table 3. A preliminary assessment will shed light on the causes for such high inaccuracies, which can be enumerated as:

1. The database of Kim and Mudawar [44] has few data with high reduced pressure as the majority of points are concentrated in the low reduced pressure range, thus over-concentrating the model.
2. The database of Kim and Mudawar [44] encompasses experimental data of water which possesses unique flow boiling mechanism owing to its high critical point and low density of vapor phase compared to synthetic and natural refrigerants such as CO_2 and propane. Presence of such data is surmised to interfere with model's capability to correctly generalize itself for all cases as the data will be rendered to be over diversified.
3. Cheng et al. [45], essentially constructed a model to predict the flow patterns of flow boiling in which after a region of annular flow when liquid thickness diminishes a dry-out area is considered. Their model was verified on the dataset of Gasche [32] and most flow patterns where correctly predicted. However, among the flow patterns there was no data point corresponding to the dry-out region.
4. The equation of Cheng et al. [45] is a modification of a previous model by Wojtan et al. [47] which was based on void fraction measurements to establish a flow pattern map. However, the study was conducted for tubes of large diameters (≅ 13mm), perhaps such a discrepancy in diameters of the original model impacted the capability of the model.
5. The expression of Ducolumbier et al. [27], while possesses a simplicity which makes its use easier, it clearly neglects to consider all the forces involved in the two-phase mechanism since it only includes the reduced pressure and the boiling number without considering the inertial and capillary forces.

Since Fig. 6 clearly demonstrates vast variations of accuracy for different values of vapor quality at the incipience of dry-out, it becomes important to delve into various experimental conditions to assess whether the erroneous predictions belong to specific experimental conditions. Therefore, the subtraction of predicted value of vapor quality and the experimental one is plotted versus reduced pressure, mass flux, diameter, heat flux and vapor quality of dry-out for each model in Fig. 7. Lines at ± 0.25 and ± 0.5 are plotted as well to have a grasp of the range in which subtraction of predictions to experimental values reside.

Considering the detailed figures, while the accuracy of predictions is randomly distributed for what concerns the reduced pressure and tube diameter, the predictions become particularly unbalanced for larger diameters, higher mass flux and heat flux. All the models suffer from large inaccuracies for vapor qualities of dry-out occurring below 0.5.

What is particularly noteworthy is the trend of subtraction of prediction to the experimental points with mass flux, where models of Kim and Mudawar [44] and Cheng et al. [45] vastly underestimate the dry-out vapor quality as opposed to Ducoulombier et al [27], which overestimates the dry-out vapor quality. This could be directly linked to the fact that Ducoulombier et al. [27], observing the duality attributed to the behavior of dry-out with increasing mass flux, decided to establish a direct relationship between the mass flux and dry-out instead of an inverse relationship established by previous authors. Therefore, with higher mass fluxes the vapor quality at the onset of dry-out increases as well in their model. However, evidently such correlation was not appropriately established as the authors only implemented a few data points. Moreover, it is worth stating that a similar trend is observed for heat fluxes as it occurs for the mass flux.

3.2. Artificial intelligence and machine learning

Over recent years there has been a rise in the number of research articles focused on flow boiling modelling with artificial neural network (ANN) and machine learning (ML). Since the research papers are diverse and concentrated on various subjects, Table 4 is constructed to comprehensively provide their findings.

Exemplary articles of Table 4 further corroborate the superiority of ML and ANN tools over the traditional empirical formulas. Despite the previous remark it must be clarified that the down side of such models is lack of an explicit equation which correlates the features with the

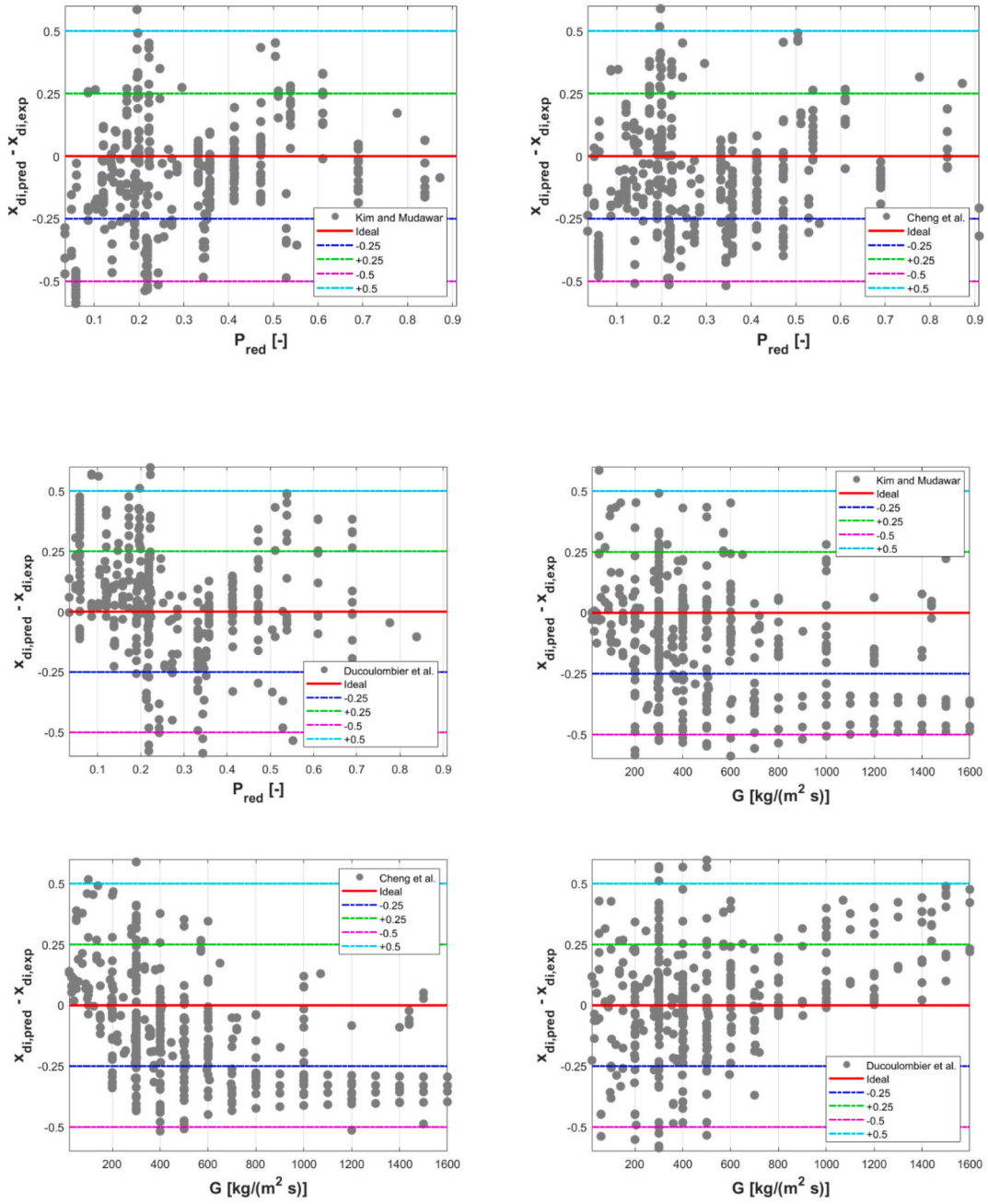

Fig. 7. Difference between predicted and experimental values of vapor quality at dry-out incipience as a function of reduced pressure, mass flux, diameter and heat flux.

outputs. Considering two models of Table 4 concerning dry-out, which is the scope of the current paper, it can be stated that no article proposes a formula which correlates the inputs and vapor quality at the incipience of dry-out. Furthermore, referring to a recent article by Loyola-Fuentes et al. [56] where recent implementation of AI in the field of heat transfer was thoroughly reviewed, the authors rightfully pointed out several downsides of such models, one of which was related to the low extrapolation capability of the models on unseen data for which an article was exemplified [57]. Loyola-Fuentes et al. [56] then proceed to introduce a framework for usage of AI modelling in the field of heat transfer.

In addition to the articles in Table 4, some new ANN works integrated with surrogate modeling are noteworthy. In these models, the neural network not only models the experimental database, but also follows physical relationships (represented through CFD simulations or empirical correlations) to predict the output for different conditions, without the need to recalculate the entire specific case. Although the methodology was not directly applied to the context of dryout incipience, some studies such as Wang et al. [58] are noteworthy; in [58] by analyzing the pressure drop and heat transfer coefficient in various U-bends the optimal geometry is found. The methodology uses a CGAN which mimics the geometrical profile and temperature profile of a CFD analysis to extrapolate and find the optimum geometry where the pressure drop is minimized and the heat transfer coefficient is maximized.

Overall, none of the built models allow the current paper to test their models on the gathered data due to absence of the explicit form of the equation.

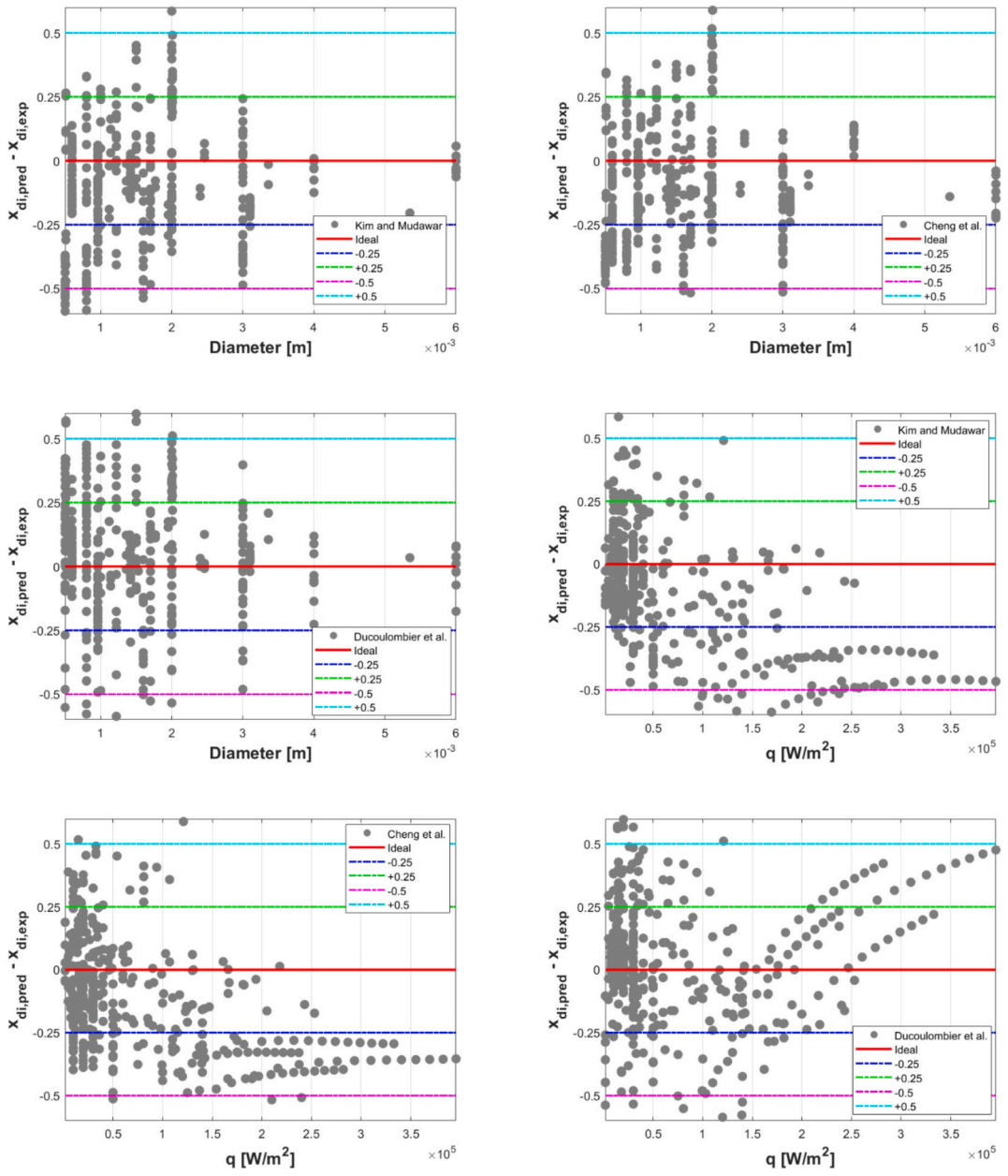

Fig. 7. (*continued*).

4. Development of a new correlation

The current paper, considering the dimensionless parameters comprehensively provided in Table 5, which presumably holistically cover all forces in two-phase flow boiling that have an impact on the onset of dry-out, suggests a new empirical correlation. The given empirical correlation has a recommended range of use in which it provides accurate results. Such a range is proportional to what has been considered in the boiling data and is enumerated as:

1. Flow boiling of HFOs, HFC/HFO mixtures, Carbon Dioxide, Propane and Ammonia.
2. Minimum and maximum acceptable diameters 0.6 mm and 3 mm (below 0.8 mm only for vertical arrangements).
3. Reduced pressures from 0.1 to 0.85.
4. Minimum and maximum acceptable heat flux 5 and 50 kW m^{-2} (for diameters below 1 mm, for the rest of the tubes, the heat fluxes presented in the database)
5. Minimum and maximum acceptable mass flux 300 and 1500 kg m^{-2} s^{-1} (mass fluxes can go as low as 150 kg m^{-2} s^{-1}, however the accuracy will substantially decrease).
6. To make sure the correlation yields the highest accuracy, we recommend consideration of the range of use, given in Appendix A for two separated parts of the model, Co > 0.4 and Co < 0.4.

The parameters in Table 5 have been implemented in many works relevant to flow boiling. The boiling number, which represents the relationship between nucleate and convective boiling, the confinement

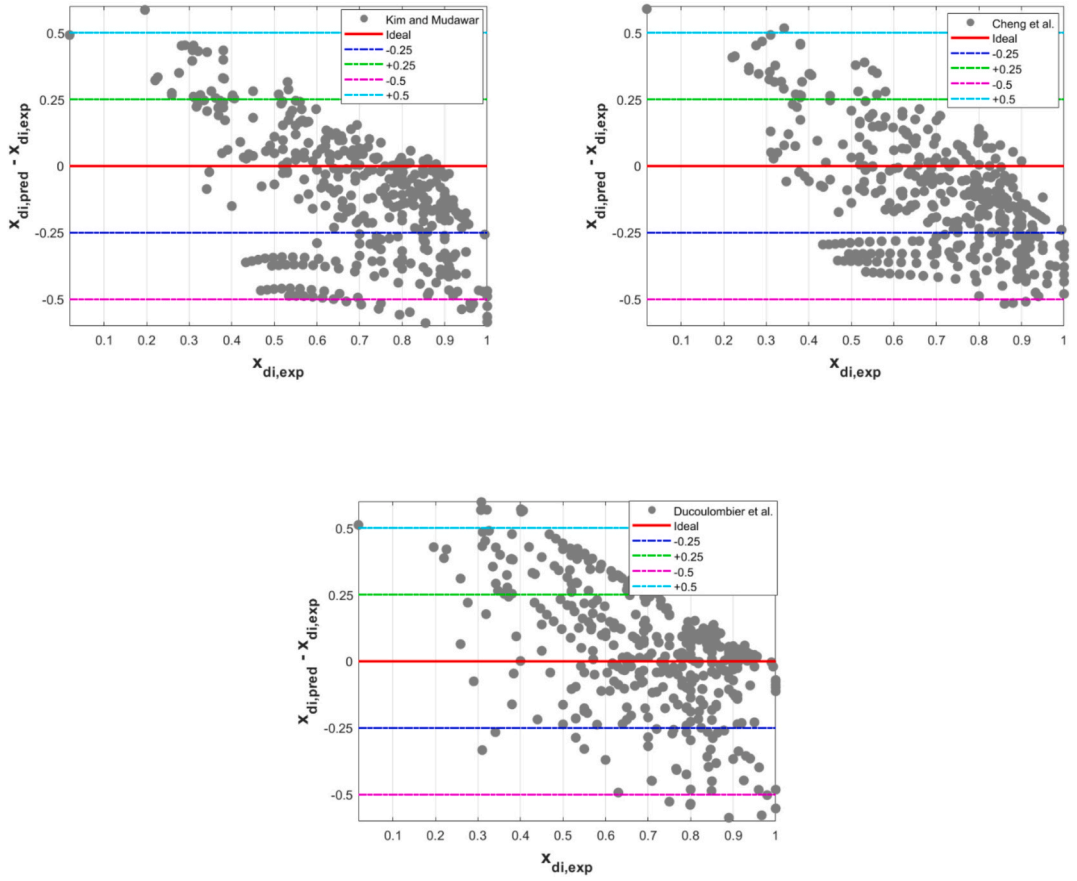

Fig. 7. (*continued*).

number, which quantifies the impact of confinement, and the reduced pressure, which directly affects nucleate boiling, could contribute to build an accurate physical model. The Weber (liquid) number, Capillary number and density ratio are added to consider the liquid thickness stability which ultimately results in annular flow transition to partial or total dryouts.

Initially the goal was to use parameters which provide a clear relationship between the forces involved in two-phase flow and avoid the RLL which is a combination of dimensionless parameters as previously suggested by Wojtan et al. [47]. However, the algorithm with RLL led to MAE improvements up to 10 %. The causality for such an occurrence is that the distribution of RLL within the dataset is quite diverse, in other words, thanks to its unique value for each operating condition, RLL statistically helps the model. The difference between the results gained with and without RLL are later on given in the current section. Moreover, it must be stated that although RLL was developed empirically, its formulation reflects key physical mechanisms governing liquid-film stability and dryout onset. The parameter combines the vapor-to-liquid density ratio, an inverse Weber term, an inverse Boiling term, and the channel diameter, effectively capturing the competition between stabilizing and destabilizing effects. Higher mass flux increases RLL by enhancing liquid-phase inertia and convective replenishment, which stabilizes the annular film despite stronger interfacial shear (the effect is multifaceted as previously discussed, depending on other conditions the corresponding increase of shear-stress forces could cause thinning of the liquid thickness). Larger channel diameters also increase RLL, as reduced confinement diminishes curvature-driven instabilities. Conversely, higher heat flux decreases RLL, consistent with faster evaporation and more rapid film thinning, while increased pressure reduces RLL due to lower surface tension and latent heat, which destabilize the film. These trends indicate that RLL, though empirical, encodes physically meaningful information about the onset of dryout, providing interpretability beyond a merely statistical correlation.

4.1. Particle Swarm optimization (PSO)

The Particle Swarm Optimization (PSO) algorithm is a population-based optimization technique inspired by the social behavior of birds flocking and fish schooling. Introduced in 1995 [61], PSO is widely used for solving complex optimization problems in various fields, including engineering, machine learning, and computational intelligence.

PSO simulates the movement of a swarm of particles in a multidimensional search space, where each particle represents a potential solution to an optimization problem. The movement of particles is influenced by the best solution found by any particle in the swarm.

Each particle updates its velocity and position based on:

A. Its previous velocity.
B. The attraction toward its pBest.
C. The attraction toward the swarm's gBest.

Mathematically, these updates are governed by the following equations:

$$v_{i(t+1)} = w \cdot v_{i(t)} + c_1 \cdot r_1 \cdot (pBest_i - x_i) + c_2 \cdot r_2 \cdot (gBest - x_i) \quad (10)$$

$$x_{i(t+1)} = x_{i(t)} + v_{i(t+1)} \quad (11)$$

where

$v_{i(t))}$ is the velocity of particle (i) at time (t).

$x_{i(t))}$ is the position of particle (i) at time (t).

(w) is the inertia weight, controlling the influence of past velocities.

(c_1) and (c_2) are acceleration coefficients that control the cognitive and social components.

(r_1) and (r_2) are random values sampled from a uniform distribution in the range $[0, 1]$.

($pBest_i$) is the best position found by particle (i) so far (personal best).

(gBest) is the best position found by any particle in the swarm (global best).

4.2. Proposed model

The parameters of Table 6 are given to an PSO algorithm with task of finding a power function that perfectly predicts the vapor quality at the incipience of dry-out. The overall form of the equation to be found is given as:

$$x_{di} = K + A \bullet We_L^a + B \bullet \rho_{ratio}^b + C \bullet Ca^c + D \bullet P_{RED}^d + E \bullet Bo^e + F \bullet Co^f + G \bullet RLL^g \quad (12)$$

PSO starts by considering combinations for exponents of (*a,b,c,d,e,f, g*) then forming a matrix including intercept (a column of ones):

$$X_{exponents} = \begin{bmatrix} 1 & (We_{L1})^a & (\rho_{ratio1})^b & (Ca_1)^c & (P_{RED1})^d & (Bo_1)^e & (Co_1)^f & (RLL_1)^g \\ 1 & (We_{L2})^a & (\rho_{ratio2})^b & (Ca_2)^c & (P_{RED2})^d & (Bo_2)^e & (Co_2)^f & (RLL_2)^g \\ 1 & (We_{L3})^a & (\rho_{ratio3})^b & (Ca_3)^c & (P_{RED3})^d & (Bo_3)^e & (Co_3)^f & (RLL_3)^g \\ \cdots & \cdots & \cdots & \cdots & \cdots & \cdots & \cdots & \cdots \\ 1 & (We_{Ln})^a & (\rho_{ration})^b & (Ca_n)^c & (P_{REDn})^d & (Bo_n)^e & (Co_n)^f & (RLL_n)^g \end{bmatrix}$$

Assuming Y is the matrix comprised of recorded experimental results.

$$Y = \begin{bmatrix} x_{di1} \\ x_{di2} \\ x_{di3} \\ \cdots \\ x_{din} \end{bmatrix}$$

β being the matrix of coefficients with K as the intercept:

$$\beta = \begin{bmatrix} K \\ A \\ B \\ C \\ D \\ E \\ F \end{bmatrix}$$

Considering:

Table 4
Research papers regard flow boiling having implemented ANN and ML models.

Articles	Number of data points	Adopted models	MAE on their data	Targeted parameter
Khalid et al. [48]	15,006 Water flow boiling	ANN KNN AdaBoost XGboost RF	8.85 % for ANN 10.39 % for XGboost	Critical Heat flux
Qiu et al. [49]	16,953 Flow boiling heat transfer in micro/mini channels	ANN	14.3 %	Heat transfer coefficient
Qiu et al. [50]	16,953 Flow boiling heat transfer in micro/mini channels	ANN	8.48 %	Heat transfer coefficient
Bard et al. [51]	16,953 Flow boiling heat transfer in micro/mini channels	Various models	11.3 % for Support vector ML	Heat transfer coefficient
Noh et al. [52]	997 Flow boiling inside micro/mini channels	XGBoost	2.45 %	Vapor quality at incipience of dry-out
Bediako and Elbargthi [53]	1578 Pre-dryout flow boiling	XGboost KNN RF ET GB	Less than 10 % for GB, XGBoost, RF and KNN for dimensional features Less than 10 % for GB, XGBoost, RF and ET for dimensionless features	Heat transfer coefficient
Afzal et al. [54]	997 flow boiling inside micro/mini channels	Guassian Process Regression	6.03 %	Vapor quality at incipience of dry-out
Irannezhad et al. [55]	1358 flow boiling inside microfin tubes	ANN	4.6 %	Heat transfer coefficient

Table 5
Parameters used for development of correlation.

Name	Formula
Boiling number	$\mathrm{Bo} = \frac{q}{G \bullet h_{lv}}$
Confinement number	$\mathrm{Co} = \frac{1}{D_h}\sqrt{\frac{\sigma}{g(\rho_L - \rho_G)}}$
Reduced pressure	$\mathrm{P_{RED}} = \frac{P_{sat}}{P_{crit}}$
Weber number (Liquid)	$\mathrm{We_L} = \frac{G^2 \bullet D_h}{\rho_L \bullet \sigma}$
Capillary number	$\mathrm{Ca} = \frac{\mu_L \bullet G}{\rho_L \bullet \sigma}$
Density ratio	$\rho_{ratio} = \frac{\rho_V}{\rho_L}$
RLL*	$\left[0.437\left(\frac{\rho_V}{\rho_L}\right)^{0.073}\left(\frac{\rho_L \bullet \sigma}{G^2}\right)^{0.24} \bullet D^{0.72} \bullet \left(\frac{G \bullet h_{lv}}{q}\right)\right]^{1/0.96}$

* Parameter by [59] derived from Wotjan et al. [60]. Unit of measure [m].

$$Y = \beta X_{exponents} \tag{13}$$

The matrix of coefficients and intercept can be solved as

$$\beta = \left(X^T X\right)^{-1} X^T Y \tag{14}$$

Having started with a supposition of the exponents and consequent calculation of coefficients with equation (13), the root mean squared error (RMSE) is evaluated as:

$$\mathrm{RMSE} = \sqrt{\frac{1}{n}\sum_{i=1}^{n}\left(y_i - \widehat{y}_i\right)^2} \tag{15}$$

where y_i will be prediction of vapor quality at the incipience of dry-out $x_{di,pred}$, and $\widehat{y}_i$ will be the target value as the experimental dry-out value $x_{di,exp}$ from the aforementioned database.

The procedure is continued by the PSO algorithm until the best global RMSE is found. Considering the explanations given thus far, the reason for which in the current context PSO is rather favorable can be given as:

A. We wish to impose a power law function between the input parameters and the vapor quality at the dryout in the form of equation (12). After selecting the exponents, Equation (14) is solved to obtain the coefficients. The relationship between the RMSE and the exponential curve can vary significantly. A PSO does not require gradients, thus eliminating the need for a well-defined Jacobian as required by other optimization algorithms.
B. We realized that Genetic algorithms (which do not have built-in mechanisms like PSO) demand extensive hyperparameter tuning, which in turn require optimization.
C. The PSO algorithm was a relatively more reasonable choice with respect to computation time requirements.
D. Given our intentions regarding the condition settings, as will be explained in connection with the Boiling number, the PSO algorithm is more favorable, since swarms that do not meet the conditions will simply not be able to displace other particles into their search space. Doing this in the context of a gradient-based optimization algorithm is significantly more complicated.

Moreover, to have a comparative assessment of optimization algorithms, several methods were tested for fitting the proposed correlation. Table 6 summarizes the results in terms of computational time, predictive accuracy (RMSE, MAE), and goodness-of-fit (R^2).

The results show that PSO and GA achieved comparable accuracy, both clearly outperforming Bayesian optimization and simulated annealing. Since all runs completed within a few minutes, computational cost is practically negligible relative to the benefits of improved predictive accuracy and robustness.

GA provided a faster solution (not considering the effort of hyperparameter tuning) with nearly identical accuracy but demonstrated slightly greater sensitivity to initialization and hyperparameters across repeated runs. Furthermore, its use was a bit more complex compared to a simple PSO algorithm. Bayesian optimization and simulated annealing offered the lowest computational times but consistently poorer accuracy, limiting their suitability for this problem.

Table 6
Performance of different optimization algorithms for model calibration.

Method	Time (s)	RMSE	MAE (%)	R^2
GA	65.47	0.1162	15.59	0.6099
PSO	112.56	0.1170	15.93	0.6101
Bayes	47.08	0.1389	21.25	0.4423
SA	45.28	0.1403	21.27	0.4312

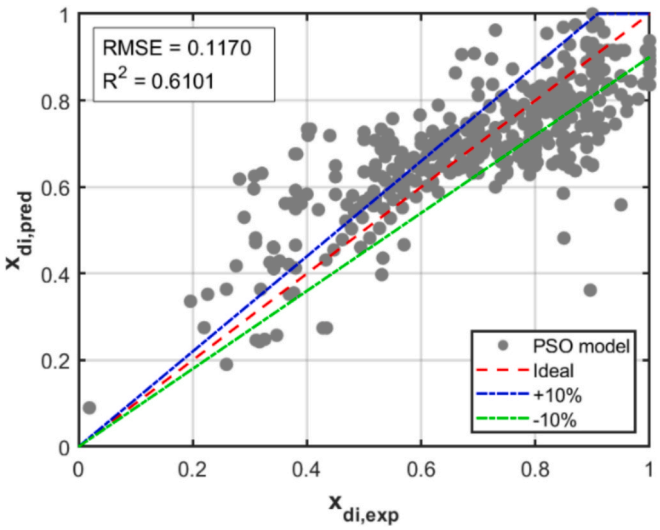

Fig. 8. Predicted values of vapor quality at the incipience of dry-out versus experimental measurements of the gathered database by the new correlation (built by PSO).

Overall, PSO was selected as the preferred optimizer because it provides the most reliable balance of accuracy, simplicity of use and robustness, and in the present context, these qualities are far more important than small differences in computational time. In reality, the goal is to produce a decent empirical correlation between the physical parameters and the phenomenon of dryout which can be achieved either through GA or PSO without notable differences.

Since the only parameter that can be inversely correlated with dry-out is heat flux, the boiling number (Bo) is forced to have a negative value for its exponent, thus $e < 0$, while the rest of the parameters are allowed to have either positive or negative exponents. The minimum RMSE value is found by a PSO model possessing the following settings which were selected using a grid search:

I. Swarm size: 1000
II. Max Iterations: 500
III. Max stall iterations: 20
IV. Function tolerance: 1e-6

Since, as previously demonstrated, the boiling mechanism varies with the tube diameter, it was proposed to discover a piecewise equation based on a suitable interval, which in turn was decided by the optimization algorithm. Such proposition comes from the stipulation that the flow patterns are considerably diverse when moving from large to smaller diameters. Moreover, as already witnessed in the exemplary works [6,30], the confinement effect alters the liquid thickness and also

Table 7
Accuracy of the new correlation.

	MAE*		
Model	Overall	$P_{RED} < 0.5$, $P_{RED} > 0.5$	$0.4 < Co < 1$
New correlation	15.93 %	15.07 %, 20.73 %	18.86 %
	$x_{di} - x_{exp}$		
New correlation	0.09	0.09, 0.1	0.11

partial and total dry-outs, thus the correlation should be diverse for those cases in which the impact of confinement begins to be pronounced. While such consideration definitely complexified the problem, the accuracy of the model was considerably increased. The new form of equation for which coefficients and the exponents were set to be optimized for a piecewise form of equation (12) based on the value of the confinement number, therefore having two RMSE values:

$$RMSE_1 = \sqrt{\frac{1}{n}\sum_{i=1}^{n}(y_i - \hat{y}_i)^2} \text{ per } Co < \text{Threshold}$$

$$RMSE_2 = \sqrt{\frac{1}{n}\sum_{i=1}^{n}(y_i - \hat{y}_i)^2} \text{ per } Co \geq \text{Threshold}$$

In this case, the PSO algorithm aims to minimize the summation of $RMSE_1$ and $RMSE_2$ while finding all the previous exponents and coefficients plus the new threshold of confinement number.

The best empirical correlation following the format of equation (12) was found to have an overall MAE of 15.93 % on the database and have the form in the table.

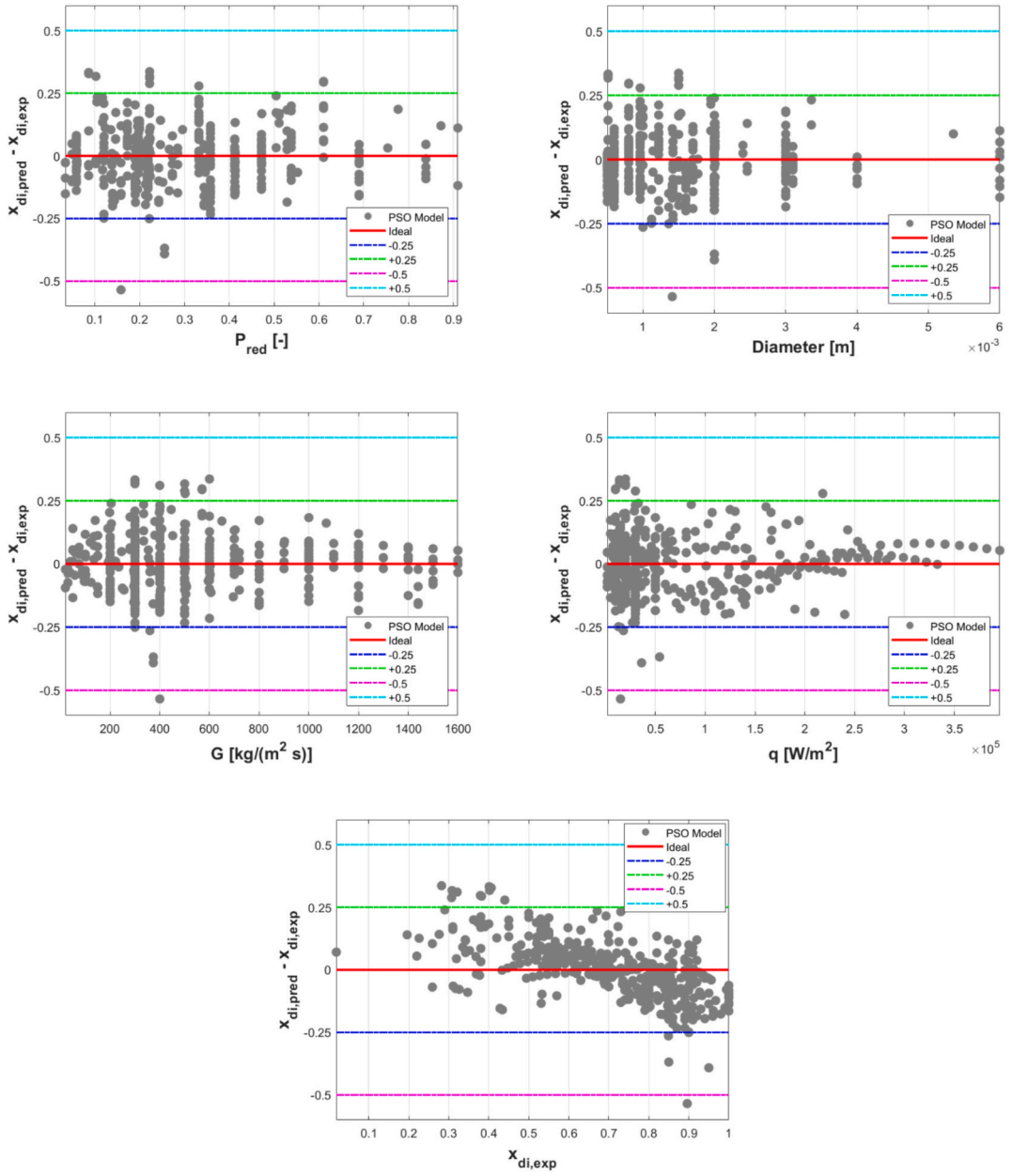

Fig. 9. Difference between predicted and experimental values of vapor quality at dry-out incipience as a function of reduced pressure, mass flux, diameter and heat flux, for the new proposed equation.

New Correlation	applicability	Eq number	Definition of parameters
$x_{di} = -0.5232 - 0.1661\,(We_L)^{0.3297} - 0.1262\,(\rho_{ratio})^{-0.7777} + 5.4037\,(Ca)^{0.2786} + 0.8708\,(P_{RED})^{-0.6686} - 5.6591\,(Co)^{2.6233} - 54.6865\,(RLL/0.01)^{-1.6477}$	Co <0.4091	Eq. (16)	$Co = \frac{1}{D_h}\sqrt{\frac{\sigma}{g(\rho_L-\rho_G)}}$, $P_{RED} = \frac{P_{sat}}{P_{crit}}$, $We_L = \frac{G^2 \bullet D_h}{\rho_L \bullet \sigma}$, $Ca = \frac{\mu_L \bullet G}{\rho_L \bullet \sigma}$, $RLL = \left[0.437\left(\frac{\rho_V}{\rho_L}\right)^{0.073}\left(\frac{\rho_L \bullet \sigma}{G^2}\right)^{0.24} \bullet D^{0.72} \bullet \left(\frac{G \bullet h_{lv}}{q}\right)\right]^{1/0.96}$, $\rho_{ratio} = \frac{\rho_V}{\rho_L}$
$x_{di} = -5.3961 - 1.0659\,(We_L)^{-0.1372} - 2.3748\,(\rho_{ratio})^{-0.2042} - 5.7707\,(Ca)^{0.2021} + 7.0818\,(P_{RED})^{-0.1352} + 0.0446\,(Bo)^{-0.3708} + 0.0110\,(Co)^{-3.2898} + 5.3964\,(RLL/0.01)^{-0.0754}$	Co $>$ 0.4091	Eq. (17)	$Bo = \frac{q}{G \bullet h_{lv}}$

In the Eqs. (16,17), *RLL* is expressed in [m] and it is divided by 0.01 m to make every part of the equation dimensionless.

The PSO algorithm finds the confinement of 0.4 to be the right threshold to provide the highest accuracy, and it is a value that was also suggested by previous authors [30] as the lower threshold of micro size definition of tubes. Another aspect regarding the provided correlation could be the absence of boiling number for low values of confinement number (corresponding to tubes larger than 2 mm, 3 mm, depending on the fluid and saturation pressure) for which the algorithm found the coefficient of 0. However, such absence does not entail that the higher boiling numbers will not impact the dry out condition as the RLL parameter has an expression of boiling number within itself. Any attempt to compare experimental data with the prediction of the proposed model should be subjected to uncertainty propagation analysis resulting from heat flux and mass flux uncertainties, according to the following equation for the estimation of the experimental uncertainty:

$$u_{x(di)} = \sqrt{\left[\left(\frac{\partial x_{\{di\}}}{\partial G}\cdot u_G\right)^2 + \left(\frac{\partial x_{\{di\}}}{\partial q}\cdot u_q\right)^2\right]} \tag{18}$$

The predictions made by the newly established correlation versus experimental values are plotted in Fig. 8. As it can be seen, considerable number of predictions reside in a 10 % error range which implies a decent predictive capability of the model. To provide further details, the MAE and absolute errors are thoroughly reported in Table 7 for the proposed correlation.

To assess the capability of the model, based on operating conditions, geometry and other features that impact the flow boiling mechanism, Fig. 9 provides the subtraction of predicted value of vapor quality and the experimental value plotted versus reduced pressure, mass flux, diameter, heat flux and dry-out vapor quality. Compared to predictions of existing empirical correlations shown in Fig. 7, the new model does not suffer from large inaccuracies with variation of parameters. Even for considerably high values of heat flux, the model still manages to keep the predictions within the 0.25 offsets. The same could be said for the diameter and the reduced pressure affecting the confinement number, for which two different correlations are used. Limited number of inaccurate predictions beyond 0.25 can be seen for low vapor qualities (below 0.4).

4.3. Testing set

To make sure the constructed model captures the flow boiling mechanism, four distinct types of data points were collected to verify the predictions of equations 16–17. The information regarding the data (133 points) is given in Table 8. All the conditions present in Table 8 were also present in the modelling phase therefore the expectation is to obtain an acceptable precision.

The predicted values of vapor quality at the incipience of dry-out versus experimental values are plotted in Fig. 10. To provide a better understanding of the reliability of predictions when varying the operating conditions of the database, the figures present classifications of diameter, reduced pressure, mass flux and refrigerant. The recorded MAE value of prediction is 14.31 % and the mean absolute error is recorded as 0.089 which is fairly acceptable despite the presence of some experimental points predicted with deviations higher than 20 %.

While predictions are fairly accurate for combination of high reduced pressures and diameters larger than 1.5 mm, the downside of the model seems to be datapoints with high reduced pressures and diameters smaller than 1.5 mm with dry-out vapor quality occurring as soon as 0.5, 0.4 and 0.3. Most of these points belong to carbon dioxide. It could also be stated that for considerably low mass fluxes less than 100 kg m^{-2} s^{-1}, and diameters larger than 1.5 mm, the model fails to provide predictions with less than 20 % of error. As evident in Fig. 10, 4 out of the 8 data

Table 8
Testing Database.

Author	Channel	d_h [mm]	Fluid	p_{RED}	G [kg m^{-2} s^{-1}]	Heating Mode	q [kW m^{-2}]	L [m]	Tube	Uncertainty x, G, q
Yun et al [62]*	SC	0.8,1, 2, 3	R744	0.41 – 0.87	58 – 1500	Electr.	1.8 – 45	0.4 – 1.2	SS	±0.04, ±0.2 %, ±5%
Shiferaw et al. [63]	SC	0.51	R134a	0.08 – 0.12	150 – 300	Electr.	14 – 29	–	SS	–
Ravellin and Thome [64]	SC	0.5 – 0.8	R134a – R245fa	0.05 – 0.21	400 – 1600	Electr.	3.2 – 422	0.110	SS	±2%, ±1%, –
Yan and Lin [65]	SC	2	R134a	0.19	50 – 200	Electr	5 – 15	–	SS	–
Callizo et al.[66] **	SC vertical	0.640	R134a R22 R245fa	0.049 – 0.238	185 – 535	Electr.	20 – 60	0.213	SS 316	±3%, ±2%, ±2%
Diani and Rossetto [67]	SC	2.5	R513A	0.17	200 – 800	Water	12 – 60	0.240	C	±0.028, ±1%,-
Lillo et al. [68]	SC	6	R32	0.29 – 0.42	300	Electr.	20 – 40	0.193	SS	±0.02, ±1%, ±0.70 %
Zhu et al. [69]	SC	2	R32	0.19	200 – 500	Electr.	10 – 30	0.4	SS	–

* The authors only tested channels with ID of 1 and 2 mm.
** Considering the diameter, the impact of verticality is expected to be diminished.

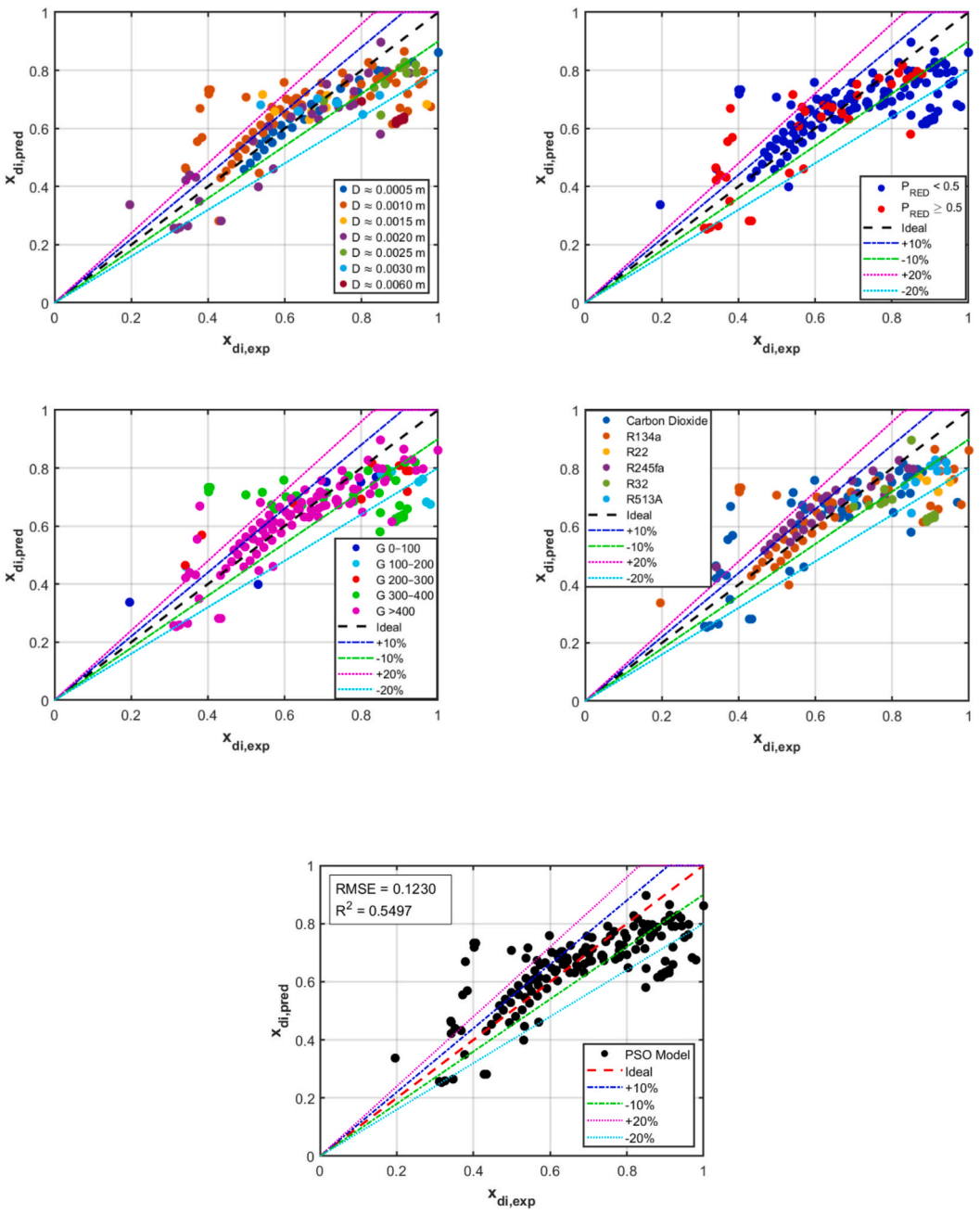

Fig. 10. Predicted values of vapor quality at the incipience of dry-out by the new correlation versus experimental values for the testing set.

Table 9
Operating conditions of points with predictions having errors beyond 35%.

G [kg / (m^2 s)]	Heat flux [W/m^2]	P_{RED} [-]	Error %	$x_{di,pred} - x_{di,exp}$
570	20,000	0.61	45	0.18
380	10,000	0.61	72	0.29
280	10,000	0.77	50	0.18
280	10,000	0.87	49	0.12
300	15,000	0.12	46	0.20
300	14,000	0.0054	87	0.33

points, taken in the 6 mm tube of Lillo et al. [68], are underestimated by more than 20 % by the model. Considering the higher frequency of small diameters within the training database and the current focus on micro and mini-sized channels, it is strongly suggested to use the model exclusively for tubes with diameters between 0.6 and 3 mm.

For a further analysis the points for which an error beyond 35 % is seen are reported in Table 9. The vapor quality at the incipience of dry-out is erroneously predicted (beyond 80 %) for data points with considerably low reduced pressure.

The other predictions which have errors beyond 35 % are mostly attributed to CO_2 at medium to high reduced pressures with high mass fluxes.

4.4. Sensitivity analysis

Since it is rather important to discern the trend behavior of the proposed model as a function of the variation of physical parameters,

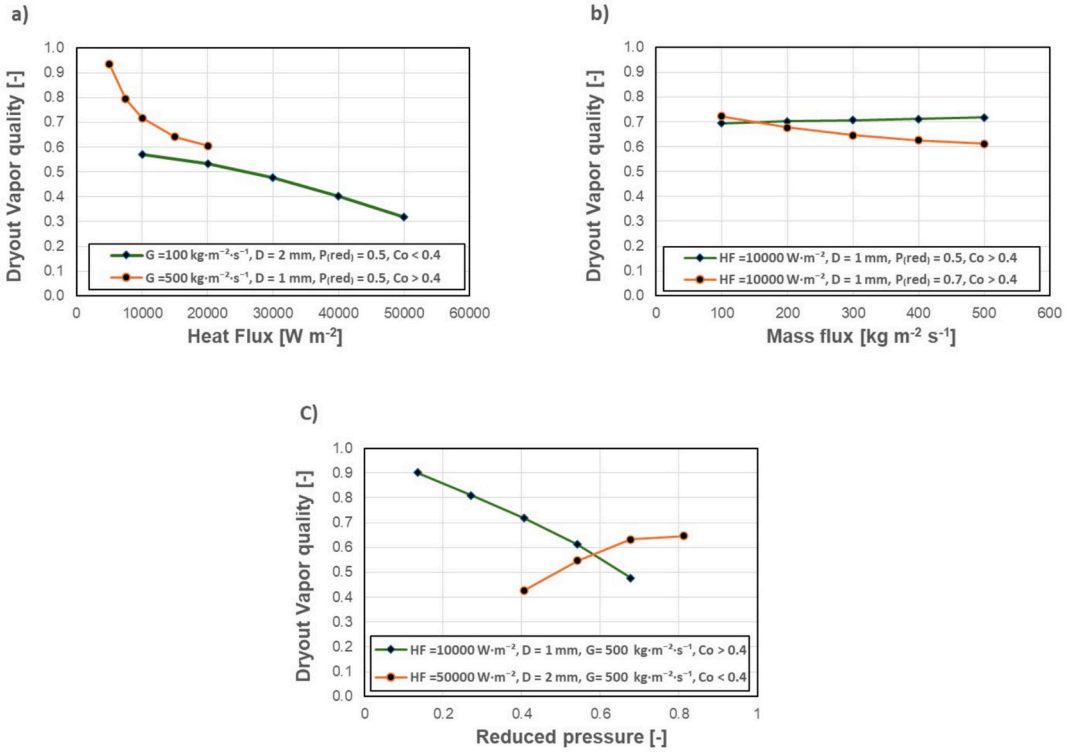

Fig. 11. Predicted CO_2 dryout vapor quality from the new model as a function of (a) heat flux, showing lower dryout vapor quality at increased heating; (b) mass flux, showing lower dryout vapor quality with higher mass rates specially at lower reduced pressures; and (c) reduced pressure, illustrating the dualistic behavior.

Table 10
Model applicability conditions.

Condition	Applicability / Range
Fluids	Flow boiling of HFOs, HFC/HFO mixtures, Carbon Dioxide, Propane, and Ammonia
Tube diameters	0.6 mm – 3 mm (below 0.8 mm only for vertical arrangements)
Reduced pressures	0.1 – 0.85
Heat flux	5 – 50 kW·m^{-2} for diameters < 1 mm; for larger tubes, heat fluxes as in the database
Mass flux	300 – 1500 kg·m^{-2}·s^{-1} (can be as low as 150 kg·m^{-2}·s^{-1}, but accuracy decreases)
Model accuracy consideration	Correlation ranges given in Appendix A, separated for Co > 0.4 and Co < 0.4

Fig. 11 is provided, which exemplifies the case of carbon dioxide. It should be noted that the operating parameters chosen are based on their availability in the database. As noted in the introductory section of the article, the relationship between mass flux and the onset of dryout has not been unilateral in the literature. It appears that the impact of mass flux, which increases the shear-stress forces that ultimately perturb the liquid thickness, can only be effective under certain circumstances. In the current model, as can be seen in Fig. 11b, the trend of dryout versus mass flux is completely reversed depending on the reduced pressure. With higher pressures and lower surface tension forces, the deformation of the liquid film around the tube becomes easier and higher mass fluxes can cause earlier dryouts. While in the opposite case, where the surface the tension is high due to low pressure, increasing the mass flux may not have a significant impact on the liquid thickness or, because it leads to a more uniform liquid thickness distribution due to higher shear forces, it may even delay drying in the upper part of the tube compared to a lower mass velocity with non-uniform liquid thickness distribution. The model also captures the dual behavior of reduced pressure, as can be seen in section C of the figure, where for tubes with confinement number below 0.4, the model predicts delayed dryouts at higher reduced pressures, due to higher vapor density and consequently low shear-stress forces, but it does exactly the opposite for the micro sizes (Co > 0.4) due to lower surface tension forces. In this case, the model predicts that higher confinement numbers are subject to much higher shear forces, which can easily lead to earlier dry-out if the surface tension force is reduced. This is not the case for larger geometries.

5. Conclusion

The current article conducts a thorough review of previous studies on dry-out phenomena inside micro and mini scale tubes for various operating conditions. Having gathered a database of vapor qualities at the incipience of dry-out and by utilization of Particle Swarm Optimization (PSO) algorithm, a new correlation was proposed which proved to give fairly accurate predictions. The model was also tested on a different database which was not implemented during the modelling phase. The outputs generated by the model could help avoid unwanted dryout conditions in real-world design applications.

Overall, the findings can be enumerated as follows:

Three empirical models were implemented to be tested on a dry-out database consisting of 418 datapoints and on average all models yielded a mean average error (MAE) of 40 %; the inaccuracy was mostly present with data with high confinement numbers as the models had MAE of 30 % for the micro scale range (0.4 < Co < 1). The inaccuracy mainly arose from the existing dissimilarity between their database which was used in the development of the model and the current one.

Using PSO, a piecewise power law function was obtained between 7 dimensionless expressions of Boiling number, Confinement number, reduced pressure, Weber number, Capillary number, density ratio and RLL; two different sets of constants are presented for confinement numbers lower or higher than 0.4.

The proposed correlation has MAE of 15.93 % and absolute error of on the modelling database. Moreover, another dataset of 133 datapoints

is used for evaluation of the correlation; with this new dataset a MAE of 14.31 % was recorded. Despite the fairly low values of MAE, which have clearly demonstrated the model's capacity, caution must be taken in the implementation of the new correlation as it should be strictly utilized for conditions reported in Table 10.

The proposed correlation is directly applicable to real-world thermal management systems where dryout critically limits performance and reliability. Relevant examples include compact evaporators in electronics cooling, CO_2-based heat pumps, and other high-flux mini-channel systems. By predicting the vapor quality at the onset of dryout over a range of channel diameters, the model provides engineers with a practical tool that can be utilized into design software and performance assessment methods. This helps significantly with optimization of channel geometry, refrigerant mass flux, and heat flux conditions while maintaining safe margins against undesirable phenomena of dryout.

In electronics cooling, such predictive capability helps prevent local temperature increase that could compromise device reliability. In CO_2-based heat pumps, it supports the design of compact and efficient evaporators by reducing the need for overly conservative safety factors. Similarly, for high-flux mini-channel applications, the correlation guides the selection of operating conditions that maximize heat transfer while avoiding premature dryout. By bridging experimental data and engineering design practice, the proposed correlation enhances the applicability of dryout onset prediction in modern two-phase thermal systems.

CRediT authorship contribution statement

Nima Irannezhad: Writing – original draft, Visualization, Investigation, Conceptualization. **Luisa Rossetto:** Writing – review & editing, Validation, Supervision, Conceptualization. **Andrea Diani:** Writing – review & editing, Validation, Supervision, Conceptualization.

Declaration of competing interest

The authors declare that they have no known competing financial interests or personal relationships that could have appeared to influence the work reported in this paper.

Appendix A

Recommended range of use for the correlation for mass flux and heat flux as inputs.

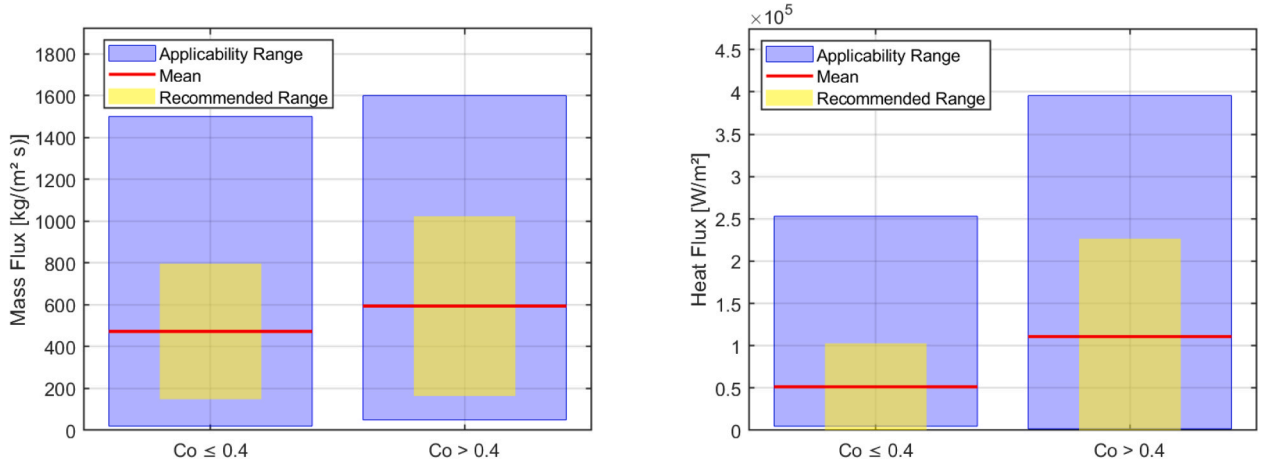

.

Data availability

Data will be made available on request.

References

[1] G.P. Celata, M. Cumo, Y. Katto, A. Mariani, Prediction of the critical heat flux in water subcooled flow boiling using a new mechanistic approach, Int. J. Heat Mass Transf. 42 (1999) 1457–1466.
[2] J.G. Collier, J.R. Thome, Convective boiling and condensation, Oxford University Press, New York, 1994.
[3] L. Cheng, D. Mewes, Review of two-phase flow and flow boiling of mixtures in small and mini channels, Int. J. Multiphase Flow 32 (2006) 183–207.
[4] S.G. Kandlikar, W.J. Grande, Evolution of microchannel flow passages—thermohydraulic performance and fabrication technology, Heat Transfer Eng. 24 (2003) 3–17.
[5] S.S. Mehendale, A.M. Jacobi, R.K. Shah, Fluid flow and heat transfer at micro-and meso-scales with application to heat exchanger design, Appl. Mech. Rev. 53 (2000) 175–193.
[6] P.A. Kew, K. Cornwell, Correlations for the prediction of boiling heat transfer in small-diameter channels, Appl. Therm. Eng. 17 (1997) 705–715.
[7] K.A. Triplett, S.M. Ghiaasiaan, S.I. Abdel-Khalik, D.L. Sadowski, Gas–liquid two-phase flow in microchannels Part I: two-phase flow patterns, Int. J. Multiphase Flow 25 (1999) 377–394.
[8] N. Brauner, D.M. Maron, Identification of the range of "small diameters" conduits, regarding two-phase flow pattern transitions, Int. Comm. Heat Mass Transf. 19 (1992) 29–39.
[9] A. Ullmann, N. Brauner, The prediction of flow pattern maps in minichannels, Multiphase, Sci. Technol. 19 (2007) 49–73.
[10] M.K. Akbar, D.A. Plummer, S.M. Ghiaasiaan, On gas–liquid two-phase flow regimes in microchannels, Int. J. Multiphase Flow 29 (2003) 855–865.
[11] W. Qu, I. Mudawar, Transport phenomena in two-phase micro-channel heat sinks, J. Electron. Packag. 126 (2004) 213–224.
[12] G.P. Celata, Single- and two-phase flow heat transfer in micropipes, In: Proceedings of the 5th Symposium, Citeseer, 2008.

[13] J. Pettersen, Two-phase flow patterns in microchannel vaporization of CO_2 at near-critical pressure, Heat Transfer Eng. 25 (2004) 52–60.
[14] R. Yun, Y. Kim, M.S. Kim, Convective boiling heat transfer characteristics of CO_2 in microchannels, Int. J. Heat Mass Transf. 48 (2005) 235–242.
[15] S. Saitoh, H. Daiguji, E. Hihara, Boiling heat transfer of R-134a flowing in horizontal small-diameter tubes, In: Heat Transfer Summer Conference, pp. 851–860, 2007.
[16] L. Chen, Y.S. Tian, T.G. Karayiannis, The effect of tube diameter on vertical two-phase flow regimes in small tubes, Int. J. Heat Mass Transf. 49 (2006) 4220–4230.
[17] Z. Anwar, B. Palm, R. Khodabandeh, Flow boiling heat transfer and dryout characteristics of R152a in a vertical mini-channel, Exp. Therm Fluid Sci. 53 (2014) 207–217.
[18] A. Arcasi, A.W. Mauro, G. Napoli, L. Viscito, Heat transfer coefficient, pressure drop and dry-out vapor quality of R454C: flow boiling experiments and assessment of methods, Int. J. Heat Mass Transf. 188 (2022) 122599.
[19] M. Pysz, S. Głuch, D. Mikielewicz, Experimental study of flow boiling pressure drop and heat transfer of R1233zd(E) at moderate and high saturation temperatures, Int. J. Heat Mass Transf. 204 (2023) 123855.
[20] D.B. Marchetto, D.C. Moreira, R. Revellin, G. Ribatski, A state-of-the-art review on flow boiling at high reduced pressures, Int. J. Heat Mass Transf. 193 (2022) 122951.
[21] R. Charnay, R. Revellin, J. Bonjour, Flow boiling heat transfer in minichannels at high saturation temperatures: Part I – experimental investigation and analysis of the heat transfer mechanisms, Int. J. Heat Mass Transf. 87 (2015) 636–652.
[22] Z. Liu, Q. Bi, Z. Yang, Y. Guo, J. Yan, Critical heat flux of cyclohexane in uniformly heated minichannels with high inlet subcooling, Exp. Therm Fluid Sci. 63 (2015) 106–114.
[23] I. Mudawar, M.B. Bowers, Ultra-high critical heat flux (CHF) for subcooled water flow boiling—I: CHF data and parametric effects for small diameter tubes, Int. J. Heat Mass Transf. 42 (1999) 1405–1428.
[24] R. Mastrullo, A.W. Mauro, L. Viscito, Flow boiling of R452A: heat transfer data, dry-out characteristics and a correlation, Exp. Therm Fluid Sci. 105 (2019) 247–260.
[25] G. Lillo, R. Mastrullo, A.W. Mauro, L. Viscito, Flow boiling heat transfer, dry-out vapor quality and pressure drop of propane (R290): experiments and assessment of predictive methods, Int. J. Heat Mass Transf. 126 (2018) 1236–1252.
[26] L. Jiang, J. Liu, L. Zhang, X. Xu, A research on the dryout characteristics of CO_2's flow boiling heat transfer process in mini-channels, Int. J. Refrig 83 (2017) 131–142.
[27] M. Ducoulombier, S. Colasson, J. Bonjour, P. Haberschill, Carbon dioxide flow boiling in a single microchannel – Part II: heat transfer, Exp. Therm Fluid Sci. 35 (2011) 597–611.
[28] S. Saitoh, H. Daiguji, E. Hihara, Correlation for boiling heat transfer of R-134a in horizontal tubes including effect of tube diameter, Int. J. Heat Mass Transf. 50 (2007) 5215–5225.
[29] R. Ali, B. Palm, Dryout characteristics during flow boiling of R134a in vertical circular minichannels, Int. J. Heat Mass Transf. 54 (2011) 2434–2445.
[30] C.L. Ong, J.R. Thome, Macro-to-microchannel transition in two-phase flow: Part 1 – two-phase flow patterns and film thickness measurements, Exp. Therm Fluid Sci. 35 (2011) 37–47.
[31] J. Pettersen, Flow vaporization of CO_2 in microchannel tubes, Exp. Therm Fluid Sci. 28 (2004) 111–121.
[32] J.L. Gasche, Carbon dioxide evaporation in a single microchannel, J. Braz. Soc. Mech. Sci. Eng. 28 (2006) 69–83.
[33] K.I. Choi, A.S. Pamitran, C.-Y. Oh, J.-T. Oh, Boiling heat transfer of R-22, R-134a, and CO_2 in horizontal smooth minichannels, Int. J. Refrig 30 (2007) 1336–1346.
[34] E. Hihara, C. Dang, Boiling heat transfer of carbon dioxide in horizontal tubes, In: ASME/JSME 2007 Thermal Engineering Heat Transfer Summer Conference, Vol. 3, ASMEDC, pp. 843–849, 2007.
[35] A.S. Pamitran, K. I. Choi, J. T. Oh, Two-phase flow boiling heat transfer and pressure drop with R-407C, R-410A, R-22, and CO_2 in horizontal minichannels, In: International Heat Transfer Conference 13, Begel House Inc., 2006.
[36] D.B. Marchetto, R. Revellin, R. Rullière, G. Ribatski, An experimental investigation on R245fa and R1233zd(E) flow boiling at high saturation temperatures in a horizontal small diameter channel, Int. J. Heat Mass Transf. 220 (2024) 124986.
[37] R. Charnay, R. Revellin, J. Bonjour, Flow boiling characteristics of R-245fa in a minichannel at medium saturation temperatures, Exp. Therm Fluid Sci. 59 (2014) 184–194.
[38] H.K. Oh, C.-H. Son, Evaporation flow pattern and heat transfer of R-22 and R-134a in small diameter tubes, Heat Mass Transf. 47 (2011) 703–717.
[39] D. Del Col, S. Bortolin, Investigation of dryout during flow boiling in a single microchannel under non-uniform axial heat flux, Int. J. Therm. Sci. 57 (2012) 25–36.
[40] J. Wu, T. Koettig, C. Franke, D. Helmer, T. Eisel, F. Haug, J. Bremer, Investigation of heat transfer and pressure drop of CO_2 two-phase flow in a horizontal minichannel, Int. J. Heat Mass Transf. 54 (2011) 2154–2162.
[41] A. Zhao, Y. Fan, Y. Suzuki, K. Morimoto, Dryout characteristics of low-GWP working fluids at low mass and heat fluxes in a vertical 4 mm diameter tube, Int. J. Heat Mass Transf. 172 (2021) 121114.
[42] Z. Anwar, B. Palm, R. Khodabandeh, Flow boiling heat transfer, pressure drop and dryout characteristics of R1234yf: experimental results and predictions, Exp. Therm Fluid Sci. 66 (2015) 137–149.
[43] M.H. Maqbool, B. Palm, R. Khodabandeh, Experimental investigation of dryout of propane in uniformly heated single vertical mini-channels, Exp. Therm Fluid Sci. 37 (2012) 121–129.
[44] S.M. Kim, I. Mudawar, Universal approach to predicting saturated flow boiling heat transfer in mini/micro-channels – Part I: dryout incipience quality, Int. J. Heat Mass Transf. 64 (2013) 1226–1238.
[45] L. Cheng, G. Ribatski, J.M. Quiben, J.R. Thome, New prediction methods for CO_2 evaporation inside tubes: Part I– A two-phase flow pattern map and a flow pattern based phenomenological model for two-phase flow frictional pressure drops, Int. J. Heat Mass Transf. 51 (2008) 111–124.
[46] R. Yun, Y. Kim, Critical quality prediction for saturated flow boiling of CO_2 in horizontal small diameter tubes, Int. J. Heat Mass Transf. 46 (2003) 2527–2535.
[47] L. Wojtan, T. Ursenbacher, J.R. Thome, Investigation of flow boiling in horizontal tubes: Part I—a new diabatic two-phase flow pattern map, Int. J. Heat Mass Transf. 48 (2005) 2955–2969.
[48] R.Z. Khalid, A. Ullah, A. Khan, M.H. Al-Dahhan, M.H. Inayat, Dependence of critical heat flux in vertical flow systems on dimensional and dimensionless parameters using machine learning, Int. J. Heat Mass Transf. 225 (2024) 125441.
[49] Y. Qiu, D. Garg, L. Zhou, C.R. Kharangate, S.M. Kim, I. Mudawar, An artificial neural network model to predict mini/micro-channels saturated flow boiling heat transfer coefficient based on universal consolidated data, Int. J. Heat Mass Transf. 149 (2020) 119211.
[50] Y. Qiu, T. Vo, D. Garg, H. Lee, C.R. Kharangate, A systematic approach to optimization of ANN model parameters to predict flow boiling heat transfer coefficient in mini/micro-channel heatsinks, Int. J. Heat Mass Transf. 202 (2023) 123728.
[51] A. Bard, Y. Qiu, C.R. Kharangate, R. French, Consolidated modeling and prediction of heat transfer coefficients for saturated flow boiling in mini/micro-channels using machine learning methods, Appl. Therm. Eng. 210 (2022) 118305.
[52] H. Noh, S. Lee, S.M. Kim, I. Mudawar, Utilization of XGBoost algorithm to predict dryout incipience quality for saturated flow boiling in mini/micro-channels, Int. J. Heat Mass Transf. 231 (2024) 125827.
[53] E.G. Bediako, A.F.A. Elbarghthi, Machine learning-based approach for predicting flow boiling heat transfer coefficient at high saturation temperatures, Int. Comm. Heat Mass Transf. 161 (2025) 108538.
[54] A. Afzal, S. Lee, S.-M. Kim, I. Mudawar, Gaussian process regression to predict dryout incipience quality of saturated flow boiling in mini/micro-channels, Appl. Therm. Eng. 256 (2024) 124137.
[55] N. Irannezhad, A. Stenger, L. Rossetto, A. Diani, Comprehensive study of flow boiling modeling inside helical micro-finned tubes: empirical, non-convex optimization and deep learning predictive models, Int. J. Heat Mass Transf. 231 (2024) 125802.
[56] J. Loyola-Fuentes, N. Nazemzadeh, E. Diaz-Bejarano, S. Mancin, F. Coletti, A framework for data regression of heat transfer data using machine learning, Appl. Therm. Eng. 248 (2024) 123043.
[57] S.S. Pai, J.A. Weibel, Machine-learning-aided design optimization of internal flow channel cross-sections, Int. J. Heat Mass Transf. 195 (2022) 123118.
[58] Q. Wang, W. Zhou, L. Yang, K. Huang, Comparison between conventional and deep learning-based surrogate models in predicting convective heat transfer performance of U-bend channels, Energy AI 8 (2022) 100140.
[59] D. Del Col, A. Cavallini, S. Bortolin, M. Matkovic, L. Rossetto, Dryout during flow boiling in a single circular minichannel: Experimentation and modelling, In: Proc. of Heat Transfer Summer Conference, Vol. 2, pp. 447-456, Paper No: HT2008-56291, 2009.
[60] L. Wojtan, R. Revellin, J. Thome, Investigation of saturated critical heat flux in a single, uniformly heated microchannel, Exp. Therm Fluid Sci. 30 (2006) 765–774.
[61] J. Kennedy, R. Eberhart, Particle swarm optimization, In: Proc. ICNN'95 – Int. Conf. Neural Networks, Vol. 4, pp. 1942–1948, 1995.
[62] R. Yun, Y. Kim, M. Soo Kim, Flow boiling heat transfer of carbon dioxide in horizontal mini tubes, Int. J. Heat Fluid Flow 26 (2005) 801–809.
[63] J. Shiferaw, M.M. Mahmoud, T.G. Karayiannis, D.B.R. Kenning, Experimental flow boiling study in a 0.52 mm diameter vertical tube using R134a, In: Proc. of 5th Eur. Therm. Sci. Conf. (2008).
[64] R. Revellin, J.R. Thome, Experimental investigation of R-134a and R-245fa two-phase flow in microchannels for different flow conditions, Int. J. Heat Fluid Flow 28 (2007) 63–71.
[65] Y.Y. Yan, T.F. Lin, Evaporation heat transfer and pressure drop of refrigerant R-134a in a small pipe, Int. J. Heat Mass Transf. 41 (1998) 4183–4194.
[66] C. Martín-Callizo, R. Ali, B. Palm, Dryout incipience and critical heat flux in saturated flow boiling of refrigerants in a vertical uniformly heated microchannel, In: ASME 2008 6th Int. Conf. Nanochannels, Microchannels, and Minichannels, pp. 705–712, 2008.
[67] A. Diani, L. Rossetto, Characteristics of R513A evaporation heat transfer inside small-diameter smooth and microfin tubes, Int. J. Heat Mass Tran. 162 (2020) 120402.
[68] G. Lillo, R. Mastrullo, A.W. Mauro, L. Viscito, Flow boiling of R32 in a horizontal stainless steel tube with 6.00 mm ID. Experiments, assessment of correlations and comparison with refrigerant R410A, Int. J. Refrig 97 (2019) 143–156.
[69] Y. Zhu, X. Wu, R. Zhao, R32 flow boiling in horizontal mini channels: Part II Flow-pattern based prediction methods for heat transfer and pressure drop, Int. J. Heat Mass Tran. 115 (2017) 1233–1244.